PHILOSOPHICAL TRANSACTIONS OF THE ROYAL SOCIETY A MATHEMATICAL, PHYSICAL & ENGINEERING SCIENCES

Electromagnetic and Hydromagnetic Waves in a Cold Magnetoplasma

H. G. Booker

Phil. Trans. R. Soc. Lond. A 1975 **280**, 57-93
doi: 10.1098/rsta.1975.0093

Phil. Trans. R. Soc. Lond. A. **280**, 57–93 (1975) [57]
Printed in Great Britain

(2) THE THEORY OF ELECTRIC AND MAGNETIC WAVES IN THE IONOSPHERE AND MAGNETOSPHERE

Electromagnetic and hydromagnetic waves in a cold magnetoplasma

By H. G. Booker
Department of Applied Physics and Information Science, University of California, San Diego, La Jolla, California 92037

The basis of the theory of waves in a cold homogeneous magnetoplasma is reviewed. The radio approximation (associated with Appleton) applies when the wave-frequency is large compared with the geometric mean of the electronic and ionic gyrofrequencies. The hydromagnetic approximation (associated with Alfvén) corresponds to infinite conductivity along the lines of flux of the imposed magnetic field and applies when the wave-frequency is small compared with the plasma-frequency. The rich variety of dispersion phenomena existing in a magnetoplasma is illustrated by polar diagrams showing both the variation of group-velocity with beam-direction and the direction in which the antenna must be pointed to aim a beam in a particular direction.

1. Introduction

The theory of waves in a cold magnetoplasma is an adaptation of a theory originally presented by H. A. Lorentz (1909) for describing the propagation of electromagnetic waves in a dielectric in the presence of a steady imposed magnetic field. As applied to a dielectric, the Lorentz theory has been superceded by a theory of the Zeeman effect based on quantum mechanics. For the free electrons in a magnetoplasma, however, classical mechanics is satisfactory. The necessary modifications and developments in the Lorentz theory were originally made principally by Appleton (1925, 1928, 1932) although others were simultaneously thinking along the same lines (Nichols & Shelleng 1925*a*, *b*; Lassen 1927; Hartree 1931).

The importance of allowing for ions as well as electrons was realized by Goubau (1935), but it was Alfvén (1942*a*, *b*, 1950) who first developed the theory of waves in a cold magnetoplasma in a form appropriate for frequencies small compared with the ionic gyrofrequency. Alfvén's concept of hydromagnetic waves was extended to all directions of propagation and to higher frequencies (Rydbeck 1948; Astrom 1950; Booker & Dyce 1965), and it is now fully integrated with the electronic version of the theory developed for radio frequencies.

At sufficiently high frequencies the velocity of propagation tends to a constant value, namely, the free-space velocity of light c. At sufficiently low frequencies, the velocity of propagation is also intimately related to a velocity that is independent of frequency and that is known as the Alfvén velocity. Alfvén originally thought of the waves as propagating along the tubes of flux of the imposed magnetic field as though these were stretched elastic strings loaded by the plasma particles. Hence the Alfvén velocity is defined as

$$A = (T/\rho)^{\frac{1}{2}}, \tag{1}$$

where T is the tension of the tubes and ρ is their mass density, provided that these quantities are properly defined. The tension is measured per unit cross sectional area and is the excess of the stress over a uniform pressure. It is therefore

$$T = B_0^2/\mu_0, \tag{2}$$

where B_0 is the flux density of the imposed magnetic field and μ_0 is the inductivity of free space. The density of the plasma is the mass that is involved in the wave motion in each unit volume. If there are N_n neutral molecules per unit volume each of mass m_n, N_i ions per unit volume each of mass m_i and N_e electrons per unit volume each of mass m_e, then the mass density is

$$\rho = N_n m_n + N_i m_i + N_e m_e, \tag{3}$$

provided that all particles are fully involved in the wave-motion. However, we shall be interested in a situation in which the neutral molecules are not involved in the wave motion, so that the relevant mass density is

$$\rho = N_i m_i + N_e m_e. \tag{4}$$

The electronic contribution to this mass density is normally negligible, and we shall call the corresponding Alfvén velocity the ionic Alfvén velocity A_i. If we drop the electronic term in equation (4), we see from equation (1) that

$$A_i^2 = B_0^2/\mu_0 N_i m_i. \tag{5}$$

At frequencies small compared with the ionic gyrofrequency, the velocity of propagation, although not precisely equal to A_i, is nevertheless closely related to it.

At radio frequencies the ions are not taking part in the wave motion, and equation (4) is then replaced by

$$\rho = N_e m_e. \tag{6}$$

It is then possible to define an electronic Alfvén velocity A_e such that

$$A_e^2 = B_0^2/\mu_0 N_e m_e, \tag{7}$$

which has some utility in discussing propagation at radio frequencies.

2. Tensor properties of a magnetoplasma

Suppose that, for a typical particle species in a plasma, there are N particles per unit volume, each having a mass m and a charge q. Let them be oscillating with angular frequency ω under the influence of an oscillating electromagnetic field for which the complex electric vector is $\boldsymbol{E}$, and let there be a steady imposed magnetic field of flux density $\boldsymbol{B}_0$. Let the resulting coherent complex oscillatory displacement of a group of particles at time t be $\boldsymbol{r}$.

Since we are discussing a cold plasma, we disregard all forces arising from gradient of gas-pressure. However, we assume that the charged particles are subject to an average collisional force proportional to their drift velocity. We can take this force as

$$-m\nu\dot{\boldsymbol{r}} \tag{8}$$

and we can describe ν as the collisional frequency for the species of charged particles under consideration. This quantity is most simply regarded as a collisional frequency with neutral particles that are not participating in the oscillatory motion. However, the effect of the collisions of electrons with ions is not excluded.

We disregard all non-linear forces, and take the averaged equation of motion for the particle species as

$$m\ddot{\boldsymbol{r}} = q(\boldsymbol{E} + \dot{\boldsymbol{r}} \times \boldsymbol{B}_0) - m\nu\dot{\boldsymbol{r}}. \tag{9}$$

For sinusoidal oscillations of angular frequency ω we introduce a harmonic time-factor $\exp(j\omega t)$. The equation of motion (9) then becomes

$$-\omega^2 m(1-j\nu/\omega)\,\boldsymbol{r} = q(\boldsymbol{E}+j\omega\boldsymbol{r}\times\boldsymbol{B}_0). \tag{10}$$

In the absence of collisions, equation (10) becomes

$$-\omega^2 m\boldsymbol{r} = q(\boldsymbol{E}+j\omega\boldsymbol{r}\times\boldsymbol{B}_0). \tag{11}$$

We may notice, however, that equation (10) may be recovered from equation (11) by replacing

$$m \quad \text{by} \quad m(1-j\nu/\omega). \tag{12}$$

It follows that we can write the equation of motion in the collisionless form (11), and still recover the effect of collisions, when needed, by employing the replacement (12). For sinusoidal oscillations the process of allowing for a collisional force of the type described by expression (8) simply corresponds to using an appropriate complex value for the particle mass.

The contribution of the particle-species to the complex electric moment per unit volume is

$$\boldsymbol{P} = Nq\boldsymbol{r}, \tag{13}$$

and in terms of this, equation (11) may be written

$$\boldsymbol{P} - j\boldsymbol{P}\times\frac{\boldsymbol{\omega}_M}{\omega} = -\frac{\omega_N^2}{\omega^2}\epsilon_0\boldsymbol{E}, \tag{14}$$

where

$$\omega_N^2 = Nq^2/\epsilon_0 m, \tag{15}$$

$$\boldsymbol{\omega}_M = q\boldsymbol{B}_0/m. \tag{16}$$

The quantity ω_N is the angular plasma frequency for the species, and $|\omega_M|$ is the angular gyrofrequency.

Let us now use cartesian coordinates (x, y, z) for which the z axis is in the direction of the imposed magnetic field. The linear algebraic equations (14) for the cartesian components of $\boldsymbol{P}$ may then be solved to obtain

$$\boldsymbol{P} = \begin{pmatrix} \kappa_T & \kappa_H & 0 \\ -\kappa_H & \kappa_T & 0 \\ 0 & 0 & \kappa_L \end{pmatrix}\epsilon_0\boldsymbol{E}, \tag{17}$$

where

$$\kappa_L = -\frac{\omega_N^2}{\omega^2}, \tag{18}$$

$$\kappa_T = \frac{\omega_N^2}{\omega_M^2-\omega^2}, \tag{19}$$

$$\kappa_H = -j\frac{\omega_N^2\omega_M}{\omega(\omega_M^2-\omega^2)}. \tag{20}$$

These equations give the contributions of the particle-species to the electric susceptivity tensor of the plasma. For the total susceptivity tensor, we add the contributions for the individual species. In the case of the Hall coefficient κ_H, it is important to notice that ω_M is positive for positive particles but negative for negative particles.

Other tensor descriptions of the plasma may be obtained, if required, from the susceptivity tensor. For the dielectric tensor we add the unit tensor to the susceptivity tensor. For the

conductivity tensor we multiply the susceptivity tensor by $j\omega$ because the current in the plasma is $\dot{\boldsymbol{P}}$, so that the complex current is

$$\boldsymbol{J} = j\omega \boldsymbol{P}. \tag{21}$$

To obtain the mobility tensor for a particular particle-species we multiply the contribution of the species to the susceptivity tensor by $j\omega/Nq$.

3. The two-fluid magnetoplasma

The simplest plasma encountered is one in which there are N electrons per unit volume (subscript e, charge $-e$) and N ions per unit volume (subscript i, charge $+e$). We then have electronic and ionic plasma frequencies defined by

$$\omega_{\mathrm{Ne}}^2 = \frac{Ne^2}{\epsilon_0 m_{\mathrm{e}}}, \quad \omega_{\mathrm{Ni}}^2 = \frac{Ne^2}{\epsilon_0 m_{\mathrm{i}}}, \tag{22}$$

and electronic and ionic gyrofrequencies defined by

$$\omega_{\mathrm{Me}} = \frac{\mathrm{e}B_0}{m_{\mathrm{e}}}, \quad \omega_{\mathrm{Mi}} = \frac{\mathrm{e}B_0}{m_{\mathrm{i}}}. \tag{23}$$

Notice that ω_{Me} has been defined to be positive so that, for electrons, ω_{M} in equation (20) is to be replaced by $-\omega_{\mathrm{Me}}$ whereas, for ions, ω_{M} is to be replaced by $+\omega_{\mathrm{Mi}}$. Notice also that

$$\frac{\omega_{\mathrm{Ne}}^2}{\omega_{\mathrm{Me}}} = \frac{\omega_{\mathrm{Ni}}^2}{\omega_{\mathrm{Mi}}} = \omega_0, \tag{24}$$

where ω_0 is an angular frequency that is characteristic of the magnetoplasma but is independent of the particle masses.

Both the electronic and ionic plasma frequencies are measures of the plasma density. So also is the quantity

$$\omega_{\mathrm{N}}^2 = \omega_{\mathrm{Ne}}^2 + \omega_{\mathrm{Ni}}^2. \tag{25}$$

Whereas ω_{Ne} and ω_{Ni} are known as the electronic and ionic angular plasma frequencies, the quantity ω_{N} is known simply as the angular plasma frequency. From equations (24) and (25) we deduce that

$$\omega_{\mathrm{Ne}}^2 = \frac{\omega_{\mathrm{Me}}}{\omega_{\mathrm{Me}} + \omega_{\mathrm{Mi}}} \omega_{\mathrm{N}}^2, \tag{26}$$

$$\omega_{\mathrm{Ni}}^2 = \frac{\omega_{\mathrm{Mi}}}{\omega_{\mathrm{Me}} + \omega_{\mathrm{Mi}}} \omega_{\mathrm{N}}^2. \tag{27}$$

Since ω_{Mi} is usually about four powers of ten less than ω_{Me}, we see that ω_{Ne} is not essentially different from ω_{N} whereas ω_{Ni} is about two powers of ten smaller than ω_{N}. Numerically, the ω_{Mi} in the denominator of equations (26) and (27) can nearly always be neglected in comparison with ω_{Me}. However, for non-numerical purposes, it is inadvisable to drop the term ω_{Mi} for two reasons. First, the symmetry of the algebra between ions and electrons is helpful and should not be upset. Secondly, one sometimes wishes to study a solid-state plasma consisting of electrons and 'holes', and the equivalent masses of the two carriers are then approximately equal.

We may notice that, by replacing μ_0 in equations (5) and (7) by $(c^2/\epsilon_0)^{-1}$, these equations may be rewritten in terms of the plasma and gyrofrequencies. For the ionic Alfvén velocity we have

$$A_{\mathrm{i}} = c(\omega_{\mathrm{Mi}}/\omega_{\mathrm{Ni}}), \tag{28}$$

PHILOSOPHICAL TRANSACTIONS OF THE ROYAL SOCIETY A MATHEMATICAL, PHYSICAL & ENGINEERING SCIENCES

and for the electronic Alfvén velocity

$$A_e = c(\omega_{Me}/\omega_{Ne}). \tag{29}$$

By multiplying numerator and denominator in equation (28) by $(m_i/m_e)^{\frac{1}{2}}$, or $(\omega_{Me}/\omega_{Mi})^{\frac{1}{2}}$, this equation may also be written

$$A_i = c(\omega_{Me}\omega_{Mi})^{\frac{1}{2}}/\omega_N. \tag{30}$$

Equation (30) is in fact preferable to equation (28) in that it corresponds to retaining the electronic term in equation (4).

By adding the contributions from the electrons and ions, with due care concerning the sign of ω_M, we deduce from equations (18), (19) and (20) that the components of the susceptivity tensor for the two-fluid magnetoplasma are given by

$$\kappa_L = -\left(\frac{\omega_{Ne}^2}{\omega^2} + \frac{\omega_{Ne}^2}{\omega^2}\right), \tag{31}$$

$$\kappa_T = \frac{\omega_{Ne}^2}{\omega_{Me}^2 - \omega^2} + \frac{\omega_{Ni}^2}{\omega_{Mi}^2 - \omega^2}, \tag{32}$$

$$\kappa_H = j\frac{1}{\omega}\left(\frac{\omega_{Ne}^2\,\omega_{Me}}{\omega_{Me}^2 - \omega^2} - \frac{\omega_{Ni}^2\omega_{Mi}}{\omega_{Mi}^2 - \omega^2}\right). \tag{33}$$

This form of the tensor components is convenient when it is desired to recognize the separate contributions of the electrons and ions. When this is not important, however, it is usually more convenient to substitute from equations (26) and (27) into equations (31), (32) and (33) so as to obtain

$$\kappa_L = -\frac{\omega_N^2}{\omega^2}, \tag{34}$$

$$\kappa_T = \frac{\omega_N^2(\omega_{Me}\omega_{Mi} - \omega^2)}{(\omega_{Me}^2 - \omega^2)(\omega_{Mi}^2 - \omega^2)}, \tag{35}$$

$$\kappa_H = -j\frac{\omega\omega_N^2(\omega_{Me} - \omega_{Mi})}{(\omega_{Me}^2 - \omega^2)(\omega_{Mi}^2 - \omega^2)}. \tag{36}$$

The effect of collisions may be incorporated in any of the formulae of this section by means of the replacement (12). If ν_e is the electronic collisional frequency and ν_i is the ionic collisional frequency, we must replace

$$\omega_{Me} \quad \text{by} \quad \frac{\omega_{Me}}{1 - j\nu_e/\omega}, \tag{37}$$

$$\omega_{Mi} \quad \text{by} \quad \frac{\omega_{Mi}}{1 - j\nu_i/\omega}, \tag{38}$$

$$\omega_{Ne}^2 \quad \text{by} \quad \frac{\omega_{Ne}^2}{1 - j\nu_e/\omega}, \tag{39}$$

$$\omega_{Ni}^2 \quad \text{by} \quad \frac{\omega_{Ni}^2}{1 - j\nu_i/\omega}. \tag{40}$$

In accordance with equation (25), ω_N^2 is replaced by

$$\frac{\omega_{Ne}^2}{1 - j\nu_e/\omega} + \frac{\omega_{Ni}^2}{1 - j\nu_i/\omega}. \tag{41}$$

The inclusion of collisions in accordance with expression (8) therefore merely requires the use of appropriate complex values for the plasma and gyro-frequencies.

4. The radio and hydromagnetic approximations

Most of the situations that need to be studied in practice can be handled by means of two approximations. One is the radio approximation, which corresponds to regarding the ions as infinitely massive. It is obtained by dropping the ionic terms in equations (31), (32) and (33), or by putting $\omega_{M1} = 0$ in equations (34), (35) and (36). Notice from equation (35) that, in general, the condition for applicability of the radio approximation is

$$\omega \gg (\omega_{Me}\,\omega_{M1})^{\frac{1}{2}}. \tag{42}$$

The second useful approximation is the hydromagnetic approximation for which the conductivity along the lines of flux of the imposed magnetic field is assumed to be infinite. This requires that

$$\kappa_L = \infty, \tag{43}$$

or, from equation (34),

$$\omega \ll \omega_N. \tag{44}$$

Inequalities (42) and (44) show that the radio approximation is useful at sufficiently high frequencies, and the hydromagnetic approximation at sufficiently low frequencies, but that the controlling frequencies are different in the two cases. For most magnetoplasmas the ionic Alfvén velocity A_1 is small compared with c so that, from equation (30),

$$(\omega_{Me}\,\omega_{M1})^{\frac{1}{2}} \ll \omega_N. \tag{45}$$

In these circumstances the domains of validity of the radio and hydromagnetic approximations overlap. The latter may then be used up to frequencies somewhat greater than the geometric mean of the gyrofrequencies, and for higher frequencies one may switch to the radio approximation.

It should be noted that, in addition to the basic approximations (42) or (44) involved in the radio or hydromagnetic approximations, it may be possible also to make additional approximations. In particular, for the hydromagnetic approximation, it is frequently possible to assume, not only that $\omega \ll \omega_N$ but also that $\omega \ll \omega_{Me}$ and hence replace the factors $\omega_{Me}^2 - \omega^2$ in equation (35) and (36) by ω_{Me}^2. It may also be possible to assume that $\omega \ll (\omega_{Me}\,\omega_{M1})^{\frac{1}{2}}$ or that $\omega \ll \omega_{M1}$. In the limit $\omega \to 0$ as originally assumed by Alfvén, equations (34), (35) and (36) become

$$\kappa_L = \infty, \quad \kappa_T = \frac{\omega_N^2}{\omega_{Me}\,\omega_{M1}}, \quad \kappa_H = 0. \tag{46}$$

5. The relations between the electromagnetic vectors in a magnetoplasma

Neglecting the effect of bound electrons, a magnetoplasma is described by means of an essentially zero magnetic moment per unit volume, and a complex electric moment per unit volume $\boldsymbol{P}$. The latter is related to the complex electric vector $\boldsymbol{E}$ by means of the susceptivity tensor κ whose components we have calculated as a function of the angular frequency ω. The constitutive relations for the plasma are then given by

$$\boldsymbol{D} = \epsilon_0 \boldsymbol{E} + \boldsymbol{P} \tag{47}$$

and

$$\boldsymbol{H} = (1/\mu_0)\,\boldsymbol{B}, \tag{48}$$

where $\boldsymbol{D}$ is the complex electric-flux-density vector, $\boldsymbol{B}$ is the complex magnetic-flux-density vector omitting the steady uniform imposed magnetic field of flux density $\boldsymbol{B}_0$, and $\boldsymbol{H}$ is

the complex magnetic vector corresponding to $\boldsymbol{B}$. These vectors are related by Maxwell's equations

$$\left.\begin{aligned} \nabla \times \boldsymbol{E} &= -\partial \boldsymbol{B}/\partial t, \quad & \nabla \cdot \boldsymbol{B} &= 0, \\ \nabla \times \boldsymbol{H} &= \partial \boldsymbol{D}/\partial t, & \nabla \cdot \boldsymbol{D} &= 0. \end{aligned}\right\} \tag{49}$$

We consider a wave in the plasma represented by an exponential wavefunction and described by means of a propagation vector $\boldsymbol{k}$. It will be convenient to use the refractive index vector $\boldsymbol{n}$, which is the ratio of $\boldsymbol{k}$ to the propagation constant ω/c in free space, so that

$$\boldsymbol{k} = (\omega/c)\,\boldsymbol{n}. \tag{50}$$

At time t at position-vector $\boldsymbol{r}$ the wavefunction is

$$\exp\{\mathrm{j}\omega(t-(1/c)\,\boldsymbol{n}\cdot\boldsymbol{r})\}. \tag{51}$$

Since all complex electromagnetic vectors are assumed to be products of this wave function with constant complex vectors, it follows that

$$\partial/\partial t \equiv \mathrm{j}\omega, \quad \nabla \equiv -\mathrm{j}(\omega/c)\,\boldsymbol{n}. \tag{52}$$

Maxwell's equations therefore become

$$\left.\begin{aligned} \boldsymbol{B} &= (1/c)\,\boldsymbol{n}\times\boldsymbol{E}, \quad & \boldsymbol{n}\cdot\boldsymbol{B} &= 0, \\ \boldsymbol{D} &= -(1/c)\,\boldsymbol{n}\times\boldsymbol{H}, & \boldsymbol{n}\cdot\boldsymbol{D} &= 0. \end{aligned}\right\} \tag{53}$$

We see from equations (53) that $\boldsymbol{B}$ and $\boldsymbol{D}$ are perpendicular to the direction of phase-propagation $\boldsymbol{n}$. We also see that the vectors $\boldsymbol{D}$, $\boldsymbol{H}$ and $\boldsymbol{n}$ form a right handed system of directions. We may notice, however, that the electric vector $\boldsymbol{E}$, although perpendicular to the common direction of $\boldsymbol{H}$ and $\boldsymbol{B}$, is not in general perpendicular to $\boldsymbol{n}$. It follows from equation (47) that the same is true of $\boldsymbol{P}$ and also of the separate contributions to $\boldsymbol{P}$ from the electrons and ions. Since the latter are proportional to the coherent displacements of the electrons and ions, it follows that the charged particles in general have a component of vibration in the direction of phase-propagation.

The arrangement of the electromagnetic vectors for a wave in a magneto-plasma is, in general, as shown in figure 1.

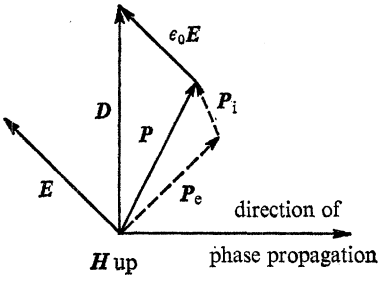

FIGURE 1. Relation between the electromagnetic vectors for a wave in a cold magnetoplasma.

6. THE DISPERSION RELATION FOR A MAGNETOPLASMA

To obtain the dispersion relation for a magnetoplasma we first eliminate $\boldsymbol{D}$, $\boldsymbol{B}$ and $\boldsymbol{H}$ from equations (53) thereby obtaining

$$\boldsymbol{P} = \epsilon_0\{(n^2-1)\,\boldsymbol{E} - (\boldsymbol{n}\cdot\boldsymbol{E})\,\boldsymbol{n}\}. \tag{54}$$

Elimination of $\boldsymbol{P}$ and $\boldsymbol{E}$ from this equation derived from Maxwell's equation, and from equation (17) derived from the particle equations of motion, then gives the dispersion relation.

The axes (x, y, z) in equation (17) were chosen so that the imposed magnetic field is in the z direction. In addition, let the yz plane now be chosen so that it contains the direction of phase propagation as shown in figure 2. Moreover, let the direction of phase-propagation make an angle θ_p with the direction of the imposed magnetic field. Then the refractive index vector is

$$\boldsymbol{n} = n(0, \sin\theta_p, \cos\theta_p) \tag{55}$$

and n is the refractive index of the magnetoplasma for a wave whose planes of constant phase are travelling in the direction $(0, \sin\theta_p, \cos\theta_p)$. Equation (54) then becomes

$$P_x = \epsilon_0(n^2 - 1)\, E_x, \tag{56}$$

$$P_y = \epsilon_0\{(n^2\cos^2\theta_p - 1)\, E_y - n^2\sin\theta_p\cos\theta_p E_z\}, \tag{57}$$

$$P_z = \epsilon_0\{-n^2\sin\theta_p\cos\theta_p E_y + (n^2\sin^2\theta_p - 1)\, E_z\}, \tag{58}$$

while equation (17) may be written

$$P_x = \epsilon_0(\kappa_T E_x + \kappa_H E_y), \tag{59}$$

$$P_y = \epsilon_0(-\kappa_H E_x + \kappa_T E_y), \tag{60}$$

$$P_z = \epsilon_0\kappa_L E_z. \tag{61}$$

Subtraction of these two sets of equations gives

$$(n^2 - 1 - \kappa_T)\, E_x - \kappa_H E_y = 0, \tag{62}$$

$$\kappa_H E_x + (n^2\cos^2\theta_p - 1 - \kappa_T)\, E_y - n^2\sin\theta_p\cos\theta_p E_z = 0, \tag{63}$$

$$-n^2\sin\theta_p\cos\theta_p E_y + (n^2\sin^2\theta_p - 1 - \kappa_L)\, E_z = 0. \tag{64}$$

Elimination of E_x, E_y and E_z then gives the dispersion relation

$$\alpha n^4 + \gamma n^2 + \epsilon = 0, \tag{65}$$

where

$$\alpha = (1 + \kappa_L) - (\kappa_L - \kappa_T)\sin^2\theta_p, \tag{66}$$

$$\gamma = -2(1 + \kappa_L)\,(1 + \kappa_T) + \{(1 + \kappa_T)\,(\kappa_L - \kappa_T) - \kappa_H^2\}\sin^2\theta_p, \tag{67}$$

$$\epsilon = (1 + \kappa_L)\,\{(1 + \kappa_T)^2 + \kappa_H^2\}. \tag{68}$$

The solution of the quadratic equation (65) for the square of the refractive index is

$$n^2 = (1 + \kappa_L)\,\frac{(1 + \kappa_T) - \kappa_H\{\frac{1}{2}\tau\sin^2\theta_p \mp (\frac{1}{4}\tau^2\sin^4\theta_p - \cos^2\theta_p)^{\frac{1}{2}}\}}{(1 + \kappa_L) - (\kappa_L - \kappa_T)\sin^2\theta_p}, \tag{69}$$

or alternatively

$$\frac{1}{n^2} = \frac{(1 + \kappa_T) - \kappa_H\{\frac{1}{2}\tau\sin^2\theta_p \pm (\frac{1}{4}\tau^2\sin^4\theta_p - \cos^2\theta_p)^{\frac{1}{2}}\}}{(1 + \kappa_T)^2 + \kappa_H^2}, \tag{70}$$

where

$$\tau = \frac{(1 + \kappa_T)\,(\kappa_L - \kappa_T) - \kappa_H^2}{\kappa_H(1 + \kappa_L)}. \tag{71}$$

The state of elliptical polarization of a wave is described by the ratios $E_x : E_y : E_z$ given by equations (62), (63) and (64). From the first and last we obtain

$$\frac{E_y}{E_x} = \frac{n^2 - 1 - \kappa_T}{\kappa_H}, \tag{72}$$

and $$\frac{E_z}{E_y} = \frac{n^2 \sin\theta_p \cos\theta_p}{n^2 \sin^2\theta_p - 1 - \kappa_L}. \tag{73}$$

These polarization ratios may be evaluated by substituting into them the values of n^2 given by equation (69) or equation (70).

Alternatively, we may evaluate the elliptical polarization-ratio E_y/E_x directly by eliminating E_z and n^2 from equations (62), (63) and (64) to give the quadratic equation

$$a(E_y/E_x)^2 + b(E_y/E_x) + c = 0, \tag{74}$$

where $$a = \kappa_H\{(1+\kappa_H) - (\kappa_L - \kappa_T)\sin^2\theta_p\}, \tag{75}$$

$$b = -\{(1+\kappa_T)(\kappa_L - \kappa_T) + \kappa_H^2\}\sin^2\theta_p, \tag{76}$$

$$c = \kappa_H\{(1+\kappa_L) - (1+\kappa_T)\sin^2\theta_p\}. \tag{77}$$

The solution of this quadratic equation is

$$\frac{E_y}{E_x} = \frac{\frac{1}{2}\sin^2\theta_p\{(1+\kappa_T)(\kappa_L - \kappa_T) + \kappa_H^2\} \pm r}{\kappa_H\{(1+\kappa_L) - (\kappa_L - \kappa_T)\sin^2\theta_p\}}, \tag{78}$$

where $$r = [\tfrac{1}{4}\sin^2\theta_p\{(1+\kappa_T)(\kappa_L - \kappa_T) - \kappa_H^2\}^2 - \cos^2\theta_p \kappa_H^2(1+\kappa_L)^2]^{\frac{1}{2}}. \tag{79}$$

In terms of E_y/E_x, the corresponding refractive index is then given by (equation 62)

$$n^2 = 1 + \kappa_T + \kappa_H(E_y/E_x). \tag{80}$$

We may notice that, for the hydromagnetic approximation ($\kappa_L \to \infty$), equation (73) becomes in general

$$E_z/E_y = 0. \tag{81}$$

The polarization ellipse for the electric vector is then perpendicular to the imposed magnetic field regardless of the direction of propagation. This is because of the assumed infinite conductivity along the lines of flux of the imposed magnetic field. Also, for the hydromagnetic approximation, equations (69) and (71) become

$$n^2 = \sec^2\theta_p[(1+\kappa_T) - \kappa_H\{\tfrac{1}{2}\tau\sin^2\theta_p \mp (\tfrac{1}{4}\tau^2\sin^4\theta_p - \cos^2\theta_p)^{\frac{1}{2}}\}], \tag{82}$$

where $$\tau = (1+\kappa_T)/\kappa_H. \tag{83}$$

7. Longitudinal propagation

Propagation at any angle to the imposed magnetic field is conveniently discussed in the light of the two special cases of longitudinal propagation ($\theta_p = 0°$) and transverse propagation ($\theta_p = 90°$).

For longitudinal propagation, the solution of the quadratic equation for the refractive index becomes (equation 69)

$$n^2 = 1 + \kappa_T \pm j\kappa_H \tag{84}$$

and the polarization ratios in equations (72) and (73) become

$$E_y/E_x = \pm j \tag{85}$$

and $$E_z/E_y = 0. \tag{86}$$

PHILOSOPHICAL TRANSACTIONS OF THE ROYAL SOCIETY A MATHEMATICAL, PHYSICAL & ENGINEERING SCIENCES

Equation (86) shows that there is no electric field parallel to the direction of phase-propagation, and it then follows from figure 1 that the same is true for the $\boldsymbol{P}$ vector. All the electromagnetic wavevectors, and all coherent particle motions, are perpendicular to the direction of phase propagation for the case of longitudinal propagation. Equation (85) shows that the wave is circularly polarized. For the upper and lower sign respectively the electromagnetic wavevectors rotate left and right handed about the direction of the imposed magnetic field whichever way the wave is propagating along the field. It is convenient to call these two waves the L and R waves respectively.

If into equation (84) we substitute for κ_T and κ_H from equations (32) and (33) we obtain for the square of the refractive index for longitudinal propagation

$$n^2 = 1 - \frac{\omega_{Ne}^2}{\omega(\omega \pm \omega_{Me})} - \frac{\omega_{Ni}^2}{\omega(\omega \mp \omega_{Mi})}. \tag{87}$$

If we substitute instead from equations (35) and (36) we obtain the equivalent result

$$n^2 = 1 - \frac{\omega_N^2}{(\omega \pm \omega_{Me})(\omega \mp \omega_{Mi})}. \tag{88}$$

Typical dispersion curves for the L and R waves for longitudinal propagation are illustrated in figure 3 for the parameters

$$\omega_N^2 = 10^{-\frac{1}{2}}\omega_{Me}^2, \quad \omega_{Mi} = 10^{-4}\omega_{Me}. \tag{89}$$

Notice that the ordinate has been plotted linearly for $-1 < n^2 < 1$ and logarithmically for $n^2 > 1$ and $n^2 < -1$. There is an infinity of n^2 for the L wave at the ionic gyrofrequency and for the R wave at the electronic gyrofrequency. As $\omega \to \infty$ the refractive indices tend to unity, but as $\omega \to 0$ they tend to n_A, where (equation 88)

$$n_A^2 = 1 + \frac{\omega_N^2}{\omega_{Me}\omega_{Mi}}. \tag{90}$$

The quantity n_A is the refractive index for Alfvén waves. In accordance with equation (30) we may rewrite equation (90) as

$$n_A^2 = 1 + c^2/A_1^2. \tag{91}$$

For most magnetoplasmas $A_1 \ll c$, and equation (91) becomes approximately

$$n_A = c/A_1. \tag{92}$$

The ionic Alfvén velocity is then the velocity of propagation along the direction of the imposed magnetic field at frequencies small compared with the ionic gyrofrequency. This is a situation in which the current in the plasma is large compared with the free-space displacement current.

The radio approximation for longitudinal propagation is obtained by dropping the ionic term in equation (87) or setting ω_{Mi} equal to zero in equation (88). We obtain

$$n^2 = 1 - \omega_N^2/[\omega(\omega \pm \omega_{Me})]. \tag{93}$$

Although in general it is necessary to have $\omega \gg (\omega_{Me}\omega_{Mi})^{\frac{1}{2}}$ for applicability of the radio approximation, the condition $\omega \gg \omega_{Mi}$ is adequate for longitudinal propagation.

If we put $\theta_p = 0$ in equation (82) we reproduce equation (84). This means that, for longitudinal propagation, the hydromagnetic approximation is identical with the unapproximated theory.

PHILOSOPHICAL TRANSACTIONS OF THE ROYAL SOCIETY A MATHEMATICAL, PHYSICAL & ENGINEERING SCIENCES

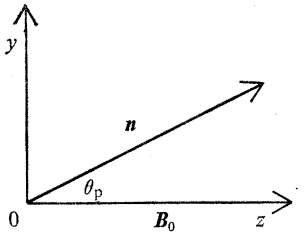

FIGURE 2. Relation between the axes of coordinates, the direction of the imposed magnetic field $\boldsymbol{B}_0$, and the direction of phase-propagation.

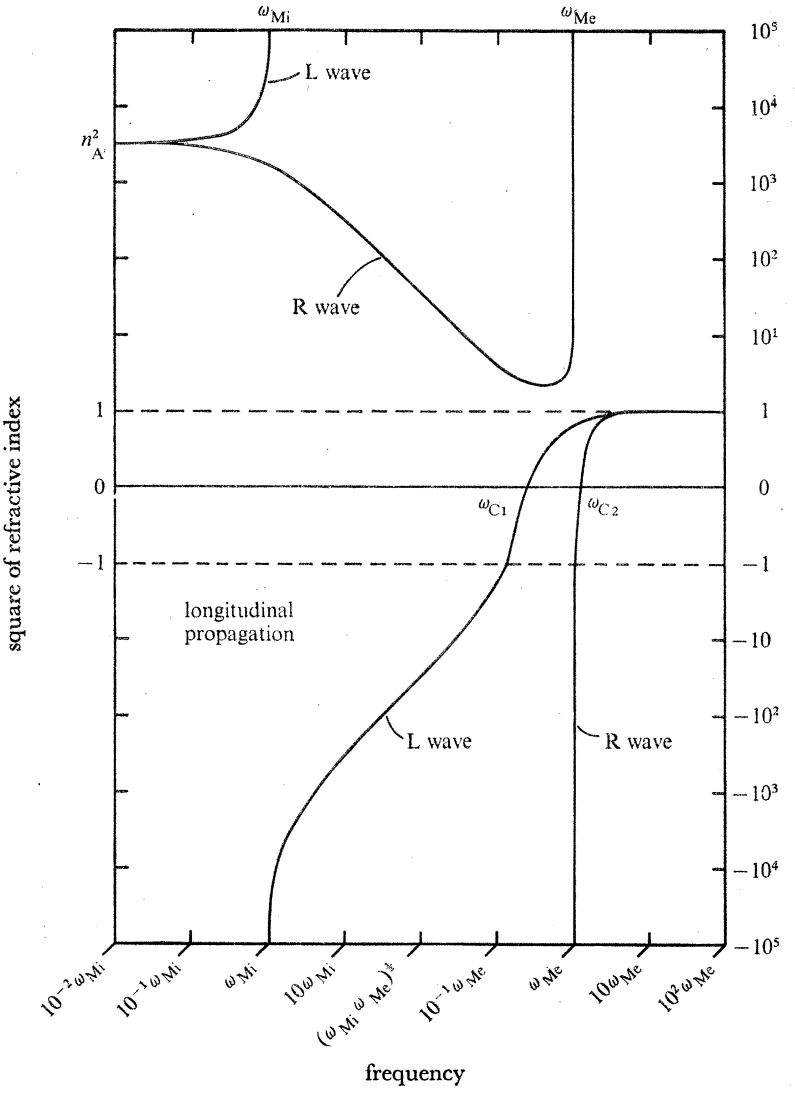

FIGURE 3. Frequency dependence of the square of refractive index for longitudinal propagation. $\omega_N^2 = 10^{-\frac{1}{2}}\omega_{Me}^2$, $\omega_{Mi} = 10^{-4}\omega_{Me}$, no collisions.

This is because the value of κ_L is irrelevant for longitudinal propagation so that the process of taking the limit $\kappa_L \to \infty$ makes no difference. However, if $\omega \ll \omega_{Me}$, equation (88) becomes

$$n^2 = 1 + \frac{\omega_N^2}{\omega_{Me}\omega_{Mi}} \frac{1}{1 \mp \omega/\omega_{Mi}} \tag{94}$$

and this reduces to equation (90) when $\omega \ll \omega_{Mi}$.

We may notice that, if equation (94) is derived from equation (87) rather than from (88), it is necessary to make use of equation (24) when combining the electronic and ionic terms. If $\omega \ll \omega_{Mi}$, the ions and electrons vibrate almost together, giving a net current that is small compared with that for the ions and electrons separately. Nevertheless this small net current is usually large compared with the free-space displacement current.

There is a wide range of frequencies for which the high frequency approximation in equation (93) and the low frequency approximation in equation (94) are both applicable, namely, $\omega_{Mi} \ll \omega \ll \omega_{Me}$. In this frequency-range both approximations become

$$n^2 = 1 \mp \omega_0/\omega, \tag{95}$$

where ω_0 is defined in equation (24). This is the Eckersley (1935) approximation used by him in seeking an explanation of whistlers.

In figure 3 there are zeros of n^2 at the critical frequencies $\omega = \omega_{C1}$ (L wave) and $\omega = \omega_{C2}$ (R wave). In accordance with equation (88), these frequencies satisfy the quadratic equation

$$\omega_N^2 = (\omega \pm \omega_{Me})(\omega \mp \omega_{Mi}) \tag{96}$$

of which the solutions are

$$\omega_{C1}, \omega_{C2} = \{\omega_N^2 + \tfrac{1}{4}(\omega_{Me} + \omega_{Mi})^2\}^{\frac{1}{2}} \mp \tfrac{1}{2}(\omega_{Me} - \omega_{Mi}). \tag{97}$$

These frequencies are usually in the radio range and may then be written with sufficient accuracy as

$$\omega_{C1}, \omega_{C2} = (\omega_N^2 + \tfrac{1}{4}\omega_{Me}^2)^{\frac{1}{2}} \mp \tfrac{1}{2}\omega_{Me}. \tag{98}$$

However, it should be noticed that, for the limit $\omega_N \to 0$, we have $\omega_{C2} \to \omega_{Me}$ but $\omega_{C1} \to \omega_{Mi}$. Notice also that

$$\omega_{C2} - \omega_{C1} = \omega_{Me} - \omega_{Mi} \doteqdot \omega_{Me} \tag{99}$$

and

$$\omega_{C1}\omega_{C2} = \omega_N^2 + \omega_{Me}\omega_{Mi}. \tag{100}$$

It may be seen from figure 3 that, for the L wave, there is a pass-band ($n^2 > 0$) for $\omega < \omega_{Mi}$ and for $\omega > \omega_{C1}$, with an intervening stop-band ($n^2 < 0$) for $\omega_{Mi} < \omega < \omega_{C1}$. For the R wave, there is a pass-band for $\omega < \omega_{Me}$ and for $\omega > \omega_{C2}$, with an intervening stop-band for $\omega_{Me} < \omega < \omega_{C2}$.

In terms of ω_{C1} and ω_{C2} the dispersion relation for longitudinal propagation may be written

$$n^2 = \frac{(\omega \mp \omega_{C1})(\omega \pm \omega_{C2})}{(\omega \mp \omega_{Mi})(\omega \pm \omega_{Me})}. \tag{101}$$

Alternatively, it may be written

$$\left(\frac{n}{n_A}\right)^2 = \frac{(1 \mp \omega/\omega_{C1})(1 \pm \omega/\omega_{C2})}{(1 \mp \omega/\omega_{Mi})(1 \pm \omega/\omega_{Me})}, \tag{102}$$

where n_A is the refractive index for Alfvén waves given by equation (90). The quantity n/n_A is the refractive index referred, not to the velocity of light c, but to the ionic Alfvén velocity A_1.

8. Transverse propagation

For propagation transverse to the imposed magnetic field we have $\theta_p = 90°$ in figure 2. The y axis is then the direction of phase propagation and the z axis is the direction of the imposed magnetic field. It is convenient to go back to equations (62), (63), and (64) which become, for $\theta_p = 90°$,

$$\frac{E_y}{E_x} = \frac{n^2 - 1 - \kappa_T}{\kappa_H} = \frac{\kappa_H}{1 + \kappa_T}, \tag{103}$$

$$(n^2 - 1 - \kappa_L)\, E_z = 0. \tag{104}$$

The two solutions are $$E_x = 0, \quad E_y = 0, \quad E_z \neq 0; \quad n^2 = 1 + \kappa_L \tag{105}$$

and $$E_x \neq 0, \quad E_y \neq 0, \quad E_z = 0; \quad n^2 = (1 + \kappa_T) + \kappa_H^2/(1 + \kappa_T). \tag{106}$$

The first solution is a wave that is linearly polarized along the imposed magnetic field and for which

$$n^2 = 1 - \omega_N^2/\omega^2. \tag{107}$$

The properties of this wave are unaffected by the imposed magnetic field, and it is known as the ordinary wave (O wave).

The second solution (equations 106) corresponds to a wave that is elliptically polarized in a plane perpendicular to the imposed magnetic field and therefore in a plane containing the direction of phase propagation. The elliptical polarization ratio in this plane is given by substituting into the last expression in equations (103) the values of κ_T and κ_H in equations (35) and (36). We obtain

$$\frac{E_y}{E_x} = -\mathrm{j}\, \frac{\omega \omega_N^2 (\omega_{Me} - \omega_{Mi})}{(\omega^2 - \omega_{Me}^2)(\omega^2 - \omega_{Mi}^2) - \omega_N^2 (\omega^2 - \omega_{Me}\omega_{Mi})}. \tag{108}$$

In the same way we find from the last of equations (106) that the square of the refractive index is

$$n^2 = 1 + \omega_N^2 \frac{\omega_N^2 - (\omega^2 - \omega_{Me}\omega_{Mi})}{(\omega^2 - \omega_{Me}^2)(\omega^2 - \omega_{Mi}^2) - \omega_N^2 (\omega^2 - \omega_{Me}\omega_{Mi})}, \tag{109}$$

or

$$n^2 = \frac{\{(\omega + \omega_{Me})(\omega - \omega_{Mi}) - \omega_N^2\}\{(\omega - \omega_{Me})(\omega + \omega_{Mi}) - \omega_N^2\}}{(\omega^2 - \omega_{Me}^2)(\omega^2 - \omega_{Mi}^2) - \omega_N^2 (\omega^2 - \omega_{Me}\omega_{Mi})}. \tag{110}$$

The properties of this wave are affected by the imposed magnetic field and it is known as the extraordinary wave (X wave).

It may be noted that the solution (106) corresponding to the X wave is independent of κ_L and consequently, for transverse propagation of the X wave, the hydromagnetic approximation ($\kappa_L \to \infty$) is identical with the exact theory. However, for transverse propagation of the O wave (solution 105), this is not true; equation (107) shows that, when ω is negligible compared with ω_N, the O wave is highly evanescent. Hence the hydromagnetic approximation makes transverse propagation of the O wave highly evanescent but correctly describes transverse propagation of the X wave. This is what would be expected for infinite conductivity along the lines of flux of the imposed magnetic field.

Typical dispersion curves for the O and X waves for transverse propagation are illustrated in figure 4 for the parameters given in equations (89). The ordinate has again been plotted linearly for $-1 < n^2 < 1$ and logarithmically for $n^2 > 1$ and $n^2 < -1$. In accordance with equation (107) there is an infinity of n^2 for the O wave at $\omega = 0$ and a zero at $\omega = \omega_N$. There are two infinities of n^2 for the X wave at $\omega = \omega_{\infty 1}$ and $\omega = \omega_{\infty 2}$, which are the zeros of the quadratic expression for

ω^2 in the denominator of equation (110). There are two zeros for the X wave at $\omega = \omega_{C1}$ and $\omega = \omega_{C2}$, which are the zeros of the numerator in equation (110). In terms of $\omega_{\infty 1}$, $\omega_{\infty 2}$, ω_{C1} and ω_{C2} the dispersion relation (110) may be written

$$n^2 = \frac{(\omega^2 - \omega_{C1}^2)(\omega^2 - \omega_{C2}^2)}{(\omega^2 - \omega_{\infty 1}^2)(\omega^2 - \omega_{\infty 2}^2)}, \tag{111}$$

and equation (108) for the polarization ratio may be written

$$\frac{E_y}{E_x} = -\mathrm{j}\,\frac{\omega\omega_N^2(\omega_{Me} - \omega_{Mi})}{(\omega^2 - \omega_{\infty 1}^2)(\omega^2 - \omega_{\infty 2}^2)}. \tag{112}$$

Figure 4 shows that there is a pass-band ($n^2 > 0$) for the O wave for $\omega > \omega_N$ and a stop-band ($n^2 < 0$) for $\omega < \omega_N$. For the X wave there is a pass-band for $\omega < \omega_{\infty 1}$, for $\omega_{C1} < \omega < \omega_{\infty 2}$, and for $\omega > \omega_{C2}$, while there are stop-bands for $\omega_{\infty 1} < \omega < \omega_{C1}$ and for $\omega_{\infty 2} < \omega < \omega_{C2}$.

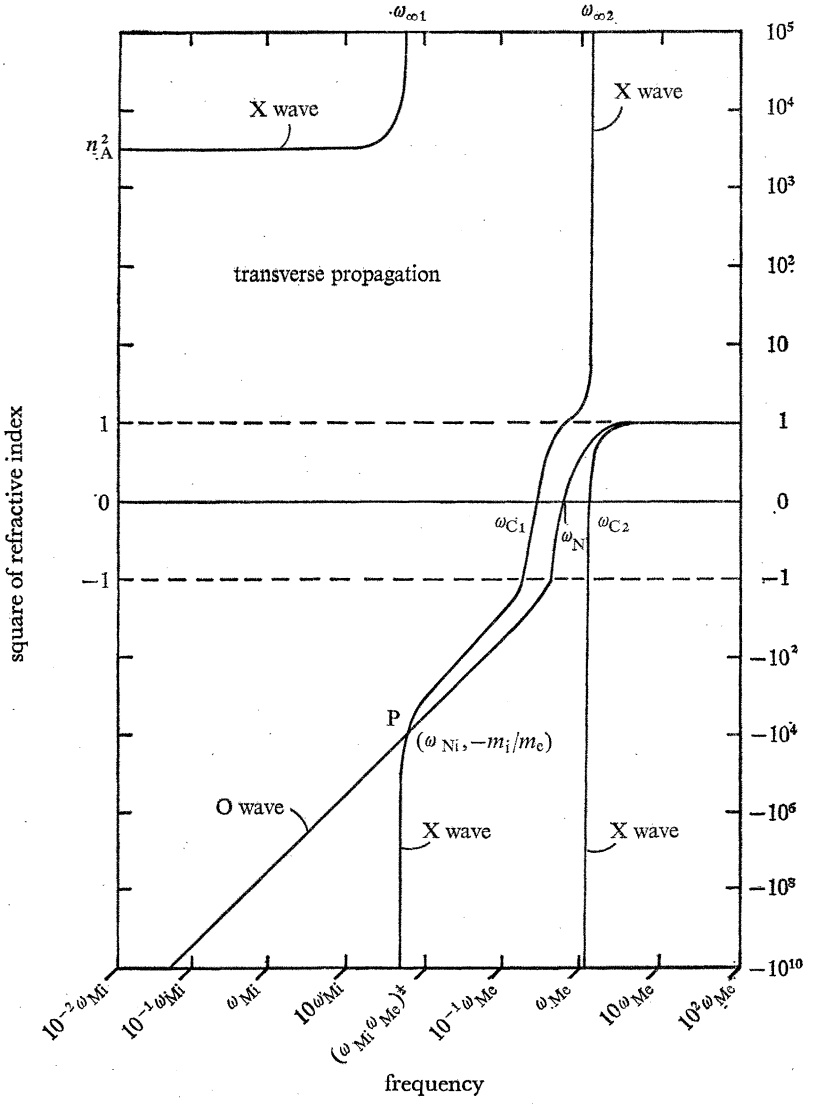

FIGURE 4. Frequency dependence of the square of refractive index for transverse propagation. $\omega_N^2 = 10^{-\frac{1}{2}}\omega_{Me}^2$, $\omega_{Mi} = 10^{-4}\omega_{Me}$, no collisions.

PHILOSOPHICAL TRANSACTIONS OF THE ROYAL SOCIETY A MATHEMATICAL, PHYSICAL & ENGINEERING SCIENCES

Equating the numerator in equation (110) to zero leads to equation (96) already encountered in connexion with longitudinal propagation. We therefore see that ω_{C1} and ω_{C2} in figure 4 have the same values as in figure 3. They are given in precise form by equation (97), or in approximate form by equation (98), and they have the properties stated in equations (99) and (100). We must notice however that, whereas ω_{C1} and ω_{C2} in figure 3 refer to different waves (the L and the R), in figure 4 they are associated with the same wave (the X). The relation between the zeros in figure 3 and those in figure 4 is an aspect of a more general property, deducible from equation (70) (Ratcliffe 1970), namely,

$$\frac{1}{n_X^2} = \frac{1}{2}\left(\frac{1}{n_L^2} + \frac{1}{n_R^2}\right), \tag{113}$$

where n_X is the refractive index for transverse propagation of the X wave and n_L, n_R are the refractive indices for longitudinal propagation of the L and R waves. From equation (113) we see that n_X vanishes both where n_L vanishes and where n_R vanishes.

From the denominator on the right hand side of equation (110) we see that the infinities of n^2 for transverse propagation of the X wave occur at angular frequencies $\omega_{\infty 1}$ and $\omega_{\infty 2}$ that satisfy the equation

$$\omega^4 - (\omega_N^2 + \omega_{Me}^2 + \omega_{Mi}^2)\,\omega^2 + (\omega_N^2 + \omega_{Me}\,\omega_{Mi})\,\omega_{Me}\,\omega_{Mi} = 0. \tag{114}$$

Hence

$$\omega_{\infty 1}^2, \omega_{\infty 2}^2 = \tfrac{1}{2}[(\omega_N^2 + \omega_{Me}^2 + \omega_{Mi}^2) \mp \{(\omega_N^2 + \omega_{Me}^2 - \omega_{Mi}^2)^2 - 4\omega_N^2\,\omega_{Mi}(\omega_{Me} - \omega_{Mi})\}^{\frac{1}{2}}]. \tag{115}$$

The quantities $\omega_{\infty 1}$ and $\omega_{\infty 2}$ are known as the lower and upper hybrid resonant angular frequencies. From equation (114) we note that

$$\omega_{\infty 1}^2 + \omega_{\infty 2}^2 = \omega_N^2 + \omega_{Me}^2 + \omega_{Mi}^2, \tag{116}$$

$$\omega_{\infty 1}^2\,\omega_{\infty 2}^2 = (\omega_N^2 + \omega_{Me}\,\omega_{Mi})\,\omega_{Me}\,\omega_{Mi}, \tag{117}$$

and, using equations (90) and (100), we further note that

$$\omega_{C1}^2\,\omega_{C2}^2 / \omega_{\infty 1}^2\,\omega_{\infty 2}^2 = n_A^2. \tag{118}$$

In the light of equation (118) it is possible to rewrite equation (111) as

$$\left(\frac{n}{n_A}\right)^2 = \frac{(1 - \omega^2/\omega_{C1}^2)\,(1 - \omega^2/\omega_{C2}^2)}{(1 - \omega^2/\omega_{\infty 1}^2)\,(1 - \omega^2/\omega_{\infty 2}^2)}. \tag{119}$$

We see therefore that, as $\omega \to 0$, the refractive index for transverse propagation of the X wave tends to the same value n_A as do the refractive indices for longitudinal propagation of the L and R waves. Figure 4 shows, however, that the same is not true for the O wave.

Because in most practical situtations $\omega_{Mi} \ll \omega_{Me}$, we can see that the radical in equation (115) is not much less than $\omega_N^2 + \omega_{Me}^2 + \omega_{Mi}^2$. Consequently the lower hybrid resonant frequency normally occurs at a relatively low frequency, while the upper hybrid resonant frequency normally occurs at a relatively high frequency.

If the upper hybrid resonant frequency is within the domain of the radio approximation, we may drop the ionic terms in equation (115) and obtain the approximate equations

$$\omega_{\infty 1} = 0, \quad \omega_{\infty 2}^2 = \omega_N^2 + \omega_{Me}^2. \tag{120}$$

In these circumstances $\omega_{\infty 1}$ may be dropped in equations (111) and (112), which then become

$$n^2 = \frac{(\omega^2 - \omega_{C1}^2)\,(\omega^2 - \omega_{C2}^2)}{\omega^2(\omega^2 - \omega_{\infty 2}^2)} \tag{121}$$

and

$$\frac{E_y}{E_x} = -\mathrm{j}\frac{\omega_N^2\,\omega_{Me}}{\omega^2(\omega^2 - \omega_{\infty 2}^2)}. \tag{122}$$

PHILOSOPHICAL TRANSACTIONS OF THE ROYAL SOCIETY A MATHEMATICAL, PHYSICAL & ENGINEERING SCIENCES

This is the form of the dispersion formulae most convenient for the X wave in the pass-bands $\omega_{C1} < \omega < \omega_{\infty 2}$ and $\omega > \omega_{C2}$ in figure 4.

When $\omega \ll \omega_{Me}$ it is convenient to return to equations (108) and (110). We drop ω in comparison with ω_{Me}, but not in comparison with $(\omega_{Me}\omega_{M1})^{\frac{1}{2}}$. From equation (110) we obtain

$$n^2 = \frac{\{(1-\omega/\omega_{M1})+\omega_N^2/\omega_{Me}\omega_{M1}\}\{(1+\omega/\omega_{M1})+\omega_N^2/\omega_{Me}\omega_{M1}\}}{(1-\omega^2/\omega_{Mi}^2)+(\omega_N^2/\omega_{Me}\omega_{M1})(1-\omega^2/\omega_{Me}\omega_{Mi})} \tag{123}$$

and from equation (108) we obtain

$$\frac{E_y}{E_x} = -\mathrm{j}\frac{(\omega_N^2/\omega_{Me}\omega_{M1})(\omega/\omega_{Mi})}{(1-\omega^2/\omega_{Mi}^2)+(\omega_N^2/\omega_{Me}\omega_{M1})(1-\omega^2/\omega_{Me}\omega_{Mi})}. \tag{124}$$

The lower hybrid resonant angular frequency $\omega_{\infty 1}$ is the value of ω for which the denominator in equations (123) and (124) vanishes. Hence

$$\omega_\infty^2 = \omega_{Mi}^2\frac{1+\omega_N^2/\omega_{Me}\omega_{Mi}}{1+\omega_N^2/\omega_{Me}^2}. \tag{125}$$

In terms of $\omega_{\infty 1}$ we may rewrite equations (123) and (124) as

$$n^2 = \frac{(1+\omega_N^2/\omega_{Me}\omega_{M1})^2-\omega^2/\omega_{Mi}^2}{(1+\omega_N^2/\omega_{Me}\omega_{M1})(1-\omega^2/\omega_{\infty 1}^2)} \tag{126}$$

and

$$\frac{E_y}{E_x} = -\mathrm{j}\frac{(\omega_N^2/\omega_{Me}\omega_{M1})(\omega/\omega_{Mi})}{(1+\omega_N^2/\omega_{Me}\omega_{M1})(1-\omega^2/\omega_{\infty 1}^2)}. \tag{127}$$

Except for a low-density plasma in which A_1 is not small compared with c, ω_N is large compared with $(\omega_{Me}\omega_{M1})^{\frac{1}{2}}$ and equations (126) and (127) may be written with sufficient accuracy as

$$\left(\frac{n}{n_A}\right)^2 = \frac{1}{(1-\omega^2/\omega_{\infty 1}^2)} \tag{128}$$

and

$$\frac{E_y}{E_y} = -\mathrm{j}\frac{\omega/\omega_{Mi}}{(1-\omega^2/\omega_{\infty 1}^2)}. \tag{129}$$

This is the form of the dispersion formulae most convenient for the X wave in the pass-band $\omega < \omega_{\infty 1}$ in figure 4.

Equation (125) for the lower hybrid resonant frequency can be restated as follows. By replacing ω_N^2 by ω_{Ne}^2 and using the first of equations (24), we may rewrite equation (125) as

$$\omega_{\infty 1}^2 = \frac{\omega_{Ni}^2+\omega_{Mi}^2}{1+\omega_{Ni}^2/\omega_{Me}\omega_{Mi}}. \tag{130}$$

For a low-density plasma, ω_N is not large compared with $(\omega_{Me}\omega_{M1})^{\frac{1}{2}}$, so that ω_{Ni} is not large compared with ω_{Mi}, and equation (130) reduces to (cf. the second of equations 120)

$$\omega_{\infty 1}^2 = \omega_{Ni}^2+\omega_{Mi}^2. \tag{131}$$

For a high density plasma we have $\omega_{Ni} \gg \omega_{Mi}$, and equation (130) reduces to

$$\omega_{\infty 1}^2 = \frac{\omega_{Ni}^2}{1+\omega_{Ni}^2/\omega_{Me}\omega_{Mi}}, \tag{132}$$

which may be rewritten

$$\frac{1}{\omega_{\infty 1}^2} = \frac{1}{\omega_{Ni}^2}+\frac{1}{\omega_{Me}\omega_{Mi}}. \tag{133}$$

PHILOSOPHICAL TRANSACTIONS OF THE ROYAL SOCIETY A MATHEMATICAL, PHYSICAL & ENGINEERING SCIENCES

showing that $\omega_{\infty 1}^2$ is one-half of the harmonic mean of ω_{Ni}^2 and $\omega_{\mathrm{Me}}\omega_{\mathrm{Mi}}$. If desired, both of the results (131) and (133) may be incorporated in the statement

$$\frac{1}{\omega_{\infty 1}^2} = \frac{1}{\omega_{\mathrm{Ni}}^2 + \omega_{\mathrm{Mi}}^2} + \frac{1}{\omega_{\mathrm{Me}}\omega_{\mathrm{Mi}}}. \tag{134}$$

It may be noticed that the approximate expressions for $\omega_{\infty 1}$ and $\omega_{\infty 2}$ in equations (134) and the second of equations (120) do not precisely satisfy the exact equations (116) and (117). This fact may be used to obtain an improved value for $\omega_{\infty 2}$, if desired, but the additional accuracy is rarely required.

The following inequalities should be noted

$$\omega_{\mathrm{Mi}} < \omega_{\infty 1} < \omega_{\mathrm{Me}} < \omega_{\infty 2}, \tag{135}$$

$$\omega_{\infty 1} < \omega_{\mathrm{C1}} < \omega_{\infty 2} < \omega_{\mathrm{C2}}. \tag{136}$$

Moreover, it is normally true that

$$\omega_{\mathrm{Mi}} \ll \omega_{\infty 1} \ll \omega_{\mathrm{Me}}, \tag{137}$$

$$\omega_{\infty 1} \ll \omega_{\mathrm{C1}}. \tag{138}$$

However, for the limit $\omega_{\mathrm{N}} \to 0$, we have $\omega_{\infty 1} \to \omega_{\mathrm{Mi}}$, $\omega_{\mathrm{C1}} \to \omega_{\mathrm{Mi}}$, $\omega_{\infty 2} \to \omega_{\mathrm{Me}}$, and $\omega_{\mathrm{C2}} \to \omega_{\mathrm{Me}}$.

Particular interest attaches to situations in which the refractive indices for the two characteristic waves in a magnetoplasma are equal. In a non-homogenous plasma, approximate equality leads to strong coupling between the waves. Even in a homogeneous plasma equality of the two refractive indices is important because it constitutes a situation where the dispersion curves for the two waves are indistinguishable and where in consequence the connexion properties of the dispersion curves can switch. A point P where $n_{\mathrm{O}} = n_{\mathrm{X}}$ appears in figure 4, and we shall find that, for propagation not quite transverse to the imposed magnetic field, and O and X curves to the left of the point P connect respectively to the X and O curves to the right of P. By equating expressions (107) and (109) for n^2, it follows that $n_{\mathrm{O}}^2 = n_{\mathrm{X}}^2$ where

$$\omega^2 = \frac{(\omega_{\mathrm{N}}^2 + \omega_{\mathrm{Me}}\omega_{\mathrm{Mi}})\,\omega_{\mathrm{Me}}\omega_{\mathrm{Mi}}}{\omega_{\mathrm{Me}}^2 - \omega_{\mathrm{Me}}\omega_{\mathrm{Mi}} + \omega_{\mathrm{Mi}}^2}. \tag{139}$$

The common value of n^2 at this frequency is

$$n_{\mathrm{O}}^2 = n_{\mathrm{X}}^2 = 1 - \frac{\omega_{\mathrm{N}}^2(\omega_{\mathrm{Me}}^2 - \omega_{\mathrm{Me}}\omega_{\mathrm{Mi}} + \omega_{\mathrm{Mi}}^2)}{(\omega_{\mathrm{N}}^2 + \omega_{\mathrm{Me}}\omega_{\mathrm{Mi}})\,\omega_{\mathrm{Me}}\omega_{\mathrm{Mi}}}. \tag{140}$$

Usually $\omega_{\mathrm{N}} \gg (\omega_{\mathrm{Me}}\omega_{\mathrm{Mi}})^{\frac{1}{2}} \gg \omega_{\mathrm{Mi}}$, and equations (139) and (140) for equality of the refractive indices for transverse propagation then become

$$\omega = \omega_{\mathrm{Ni}}, \quad n_{\mathrm{O}}^2 = n_{\mathrm{X}}^2 = -\omega_{\mathrm{Me}}/\omega_{\mathrm{Mi}}. \tag{141}$$

These are therefore the coordinates of the point P in figure 4.

9. Quasi-longitudinal and quasi-transverse propagation

If the direction of phase-propagation in a magnetoplasma is sufficiently close to the longitudinal direction or to the transverse direction, then the phenomena of propagation are quite similar to those for $\theta_{\mathrm{p}} = 0°$ or $\theta_{\mathrm{p}} = 90°$ respectively. Propagation is then said to be either quasi-longitudinal (QL) or quasi-transverse (QT). It should be noticed, however, that far more than the numerical value of θ_{p} is involved in deciding whether propagation is QL, QT or intermediate between the two.

Propagation is QL if the $\cos^2\theta_p$ term in the radical of equation (69) predominates. It is QT if the $\frac{1}{4}\tau^2\sin^4\theta_p$ term predominates. The two terms are equal for the value of θ_p given by

$$\sin^2\theta_p/2\cos\theta_p = |\tau|, \tag{142}$$

where τ is given by equation (71). Since $|\tau|$ varies over many powers of ten, the transition value of θ_p given by equation (142) may be very close to 0° or it may be very close to 90°.

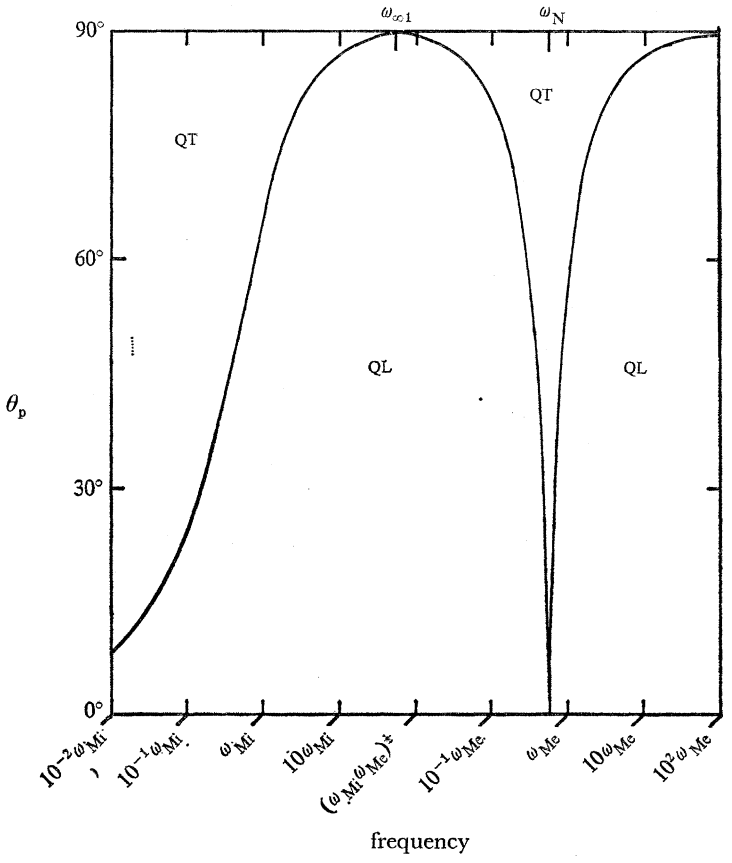

FIGURE 5. Frequency dependence of the value of θ_p for transition between quasi-longitudinal (QL) and quasi-transverse (QT) propagation. $\omega_N^2 = 10^{-\frac{1}{2}}\omega_{Me}^2$, $\omega_{Mi} = 10^{-4}\omega_{Me}$, no collisions.

The curve in figure 5 shows the values of the transition value of θ_p as a function of angular frequency for a magnetoplasma having the parameters given in equations (89). We see that, for $\omega_{Mi} \ll \omega \ll \omega_N$ and for $\omega \gg \omega_N$, propagation is QL for nearly all values of θ_p, while for $\omega \sim \omega_N$ and $\omega \ll \omega_{Mi}$ propagation is QT for nearly all values of θ_p.

For $\omega = \omega_N$ the transition from QT to QL propagation is discontinuous at $\theta_p = 0°$ unless collisions are taken into account. For $\omega = \omega_{\infty 1}$ the transition from QL to QT propagation is discontinuous at $\theta_p = 90°$ unless collisions are taken into account. For the limit $\omega \to 0$ frequently encountered in fluid mechanics literature, propagation is QT for all values of θ_p except $\theta_p = 0$. For the limit $\omega \to \infty$ frequently encountered in connexion with Faraday rotation of the plane of polarization in a relatively weak magnetoplasma, propagation is QL except for $\theta_p = 90°$.

Except in the neighbourhood of the QL/QT transition curve in figure 5, all formulae involving the radical in equation (69) may be simplified by suitable binomial expansion.

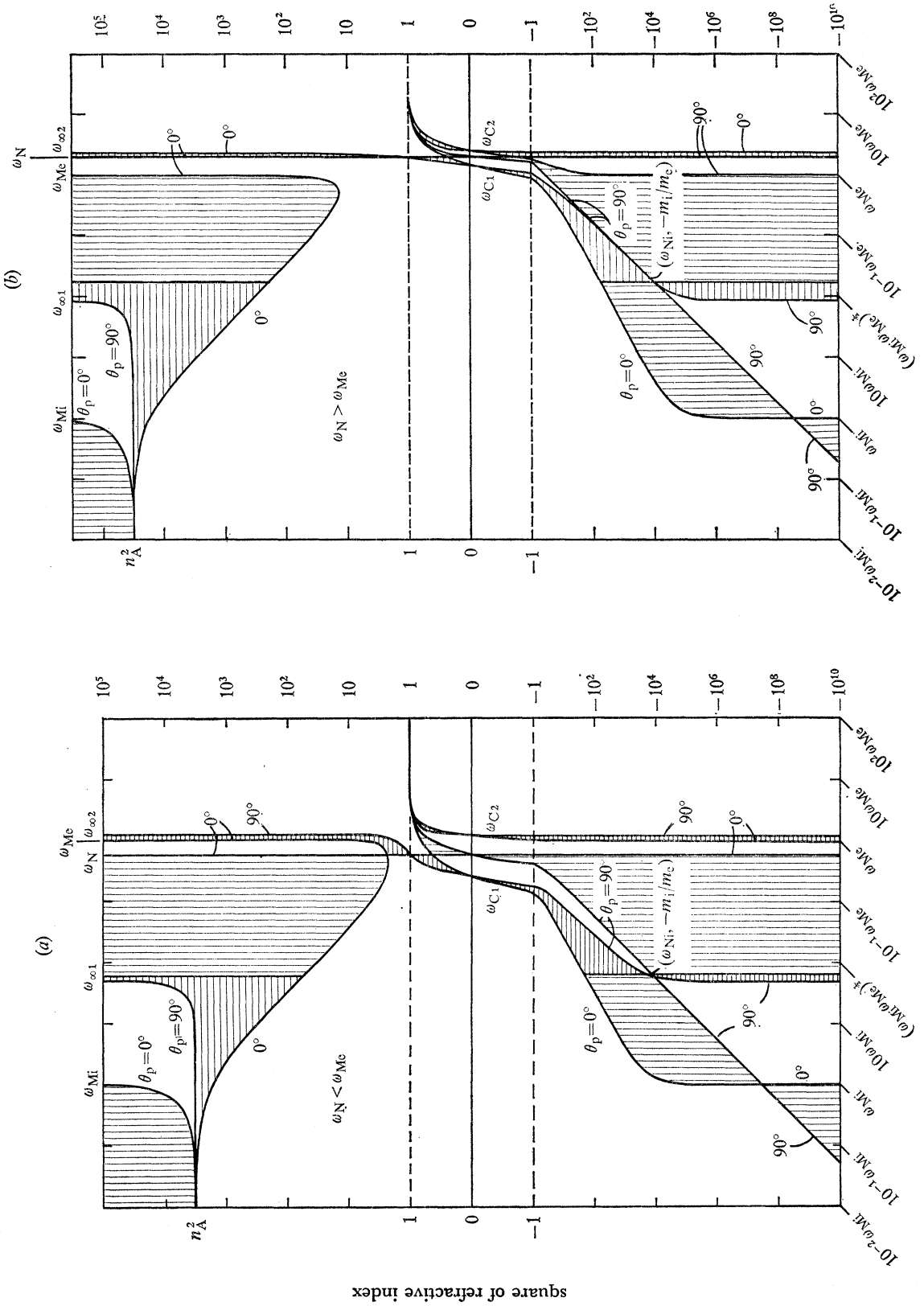

FIGURE 6*a*. Illustrating the frequency dependence of the square of refractive index for the O wave (vertical shading) and the X wave (horizontal shading). $\omega_N^2 = 10^{-\frac{1}{2}}\omega_{Me}^2$, $\omega_{Mi} = 10^{-4}\omega_{Me}$, no collisions. *b*, Illustrating the frequency dependence of the square of refractive index for the O wave (vertical shading) and the X wave (horizontal shading). $\omega_N^2 = 10^{\frac{1}{2}}\omega_{Me}^2$, $\omega_{Mi} = 10^{-4}\omega_{Me}$, no collisions.

PHILOSOPHICAL TRANSACTIONS OF THE ROYAL SOCIETY A MATHEMATICAL, PHYSICAL & ENGINEERING SCIENCES

10. Phase propagation at any fixed angle to the imposed magnetic field

To obtain curves showing n^2 as a function of ω for fixed values of θ_p other than 0° or 90° we employ a method introduced by Ratcliffe (1933, 1959). If the curves for $\theta_p = 0°$ and $\theta_p = 90°$ are drawn on the same diagram, it is then possible to shade the intervening regions in such a way as to show the location of the curves for $0° < \theta_p < 90°$.

In figure 6*a*, the longitudinal and transverse curves are copied from figures 3 and 4, and shading is suitably inserted between the two sets of curves. For one of the characterististic waves in the magnetoplasma corresponding to a fixed value of θ_p between 0° and 90° the curve for n^2 starts at $n^2 = 1$ for $\omega \gg \omega_N$, passes through the vertically shaded region, and goes through zero at $\omega = \omega_N$, It is then in a vertically shaded region corresponding to a stop-band. The curve for n^2 passes to $-\infty$ in this band, and then reappears at $n^2 = +\infty$, where we enter a pass-band. The curve then runs from a vertically shaded region into a horizontally shaded region near $\omega = \omega_{N1}$, and finally $n^2 \to n_A^2$ as $\omega \to 0$. If the selected value of θ_p is sufficiently close to 90°, the crossing from vertical to horizontal shading occurs for $n^2 < 0$.

For the other characteristic wave in the magnetoplasma, the curve for n^2 starts at $n^2 = 1$ for $\omega \gg \omega_{C2}$, passes through the horizontally shaded region, and goes through zero into a stop-band at $\omega = \omega_{C2}$. The curve for n^2 passes to $-\infty$ in the band $\omega_{Me} < \omega < \omega_{\infty 2}$ and then reappears at $n^2 = +\infty$. We are again in a pass-band, and the curve continues in the horizontally shaded region, crossing through $n^2 = 1$ at $\omega = (\omega_N^2 + \omega_{Me}\omega_{Mi})^{\frac{1}{2}} \fallingdotseq \omega_N$, and then through zero at $\omega = \omega_{C1}$. It continues through the stop-band indicated by horizontal shading, crossing into a vertically shaded region near $\omega = \omega_{N1}$. It crosses into another vertically shaded region near $\omega = \omega_{Mi}$, and then passes to $n^2 = -\infty$. The curve for n^2 reappears at $n^2 = +\infty$ in the band $\omega < \omega_{Mi}$ indicated by vertical shading, and we are again in a pass-band. The value of n^2 tends to $n_A^2 \sec^2\theta_p$ as $\omega \to 0$.

The limits of these curves as θ_p tends to 0° and 90° are shown in figure 6*a*. It should be noticed that the vertical shading is such that it terminates at $\theta_p = 90°$ on the O wave curve of figure 4, while the horizontal shading terminates at $\theta_p = 90°$ on the X wave curve of figure 4. For this reason, a curve in the vertically shaded region is usually said to correspond to an O wave regardless of the value of θ_p. Likewise a curve in the horizontally shaded region is said to correspond to an X wave. Where a curve crosses from one type of shading to the other, the name of the corresponding wave changes, and this is particularly inconvenient in a pass-band. The pass-band where this occurs in figure 6*a* is that corresponding to the whistler phenomenon (Storey 1953; Helliwell 1965). In this band the wave may be conveniently called the whistler wave.

It should be noted that figure 6*a* is drawn for $\omega_N < \omega_{Me}$. If $\omega_N > \omega_{Me}$, the shaded regions are modified slightly as shown in figure 6*b*. Figure 6*b* is drawn for $\omega_N^2 = 10^{\frac{1}{2}}\omega_{Me}^2$ rather than for $\omega_N^2 = 10^{-\frac{1}{2}}\omega_{Me}^2$. Figures 6*a* and *b* show that, in general, the pass-band for the whistler wave is $\omega < \text{Min}\,(\omega_N, \omega_{Me})$.

11. The relation between phase and group propagation

The discussion in the previous section was concerned with n^2 as a function of ω for fixed θ_p. What this implies may be understood with the aid of figure 7, where it is supposed that a pulse can be radiated from a broadside antenna located in a magnetoplasma. It should be noticed that the direction of the beam is not in general perpendicular to the aperture-plane of the antenna. What

the aperture-plane of the antenna controls is the orientation of the individual wave-crests within the pulse. A fixed value of θ_p therefore implies that the antenna is facing in a fixed direction relative to the direction of the imposed magnetic field. As the frequency varies, however, the direction of the beam in general changes.

Again, the refractive index n is the ratio of c to the velocity V_p with which the individual wave-crests within the pulse are advancing. This is not the velocity V_g with which the pulse is moving along the beam. What we have studied so far, therefore, is the way in which the velocity of the individual wave-crests varies with the direction of the antenna, not the way in which the pulse-velocity along the beam varies with the direction of the beam.

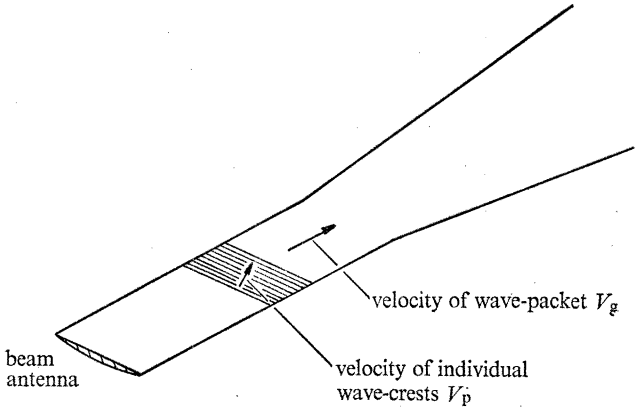

FIGURE 7. Illustrating the radiation of a pulse from a beam-antenna in a magnetoplasma.

To study the latter we have to consider a group of plane waves whose directions of phase propagation have a suitable spread, and whose frequencies also have a suitable spread. Such a group can interfere constructively in the neighbourhood of a moving point to produce a pulsed beam roughly as illustrated in figure 7. The velocity of the point of constructive interference is the group-velocity $\boldsymbol{V}_g$, and the angle θ_g that this velocity makes with the direction of the imposed magnetic field gives the group-direction, or beam-direction. We need to study V_g as a function of θ_g. In addition, for each θ_g, we need to know the corresponding value of θ_p; this gives the direction in which the antenna must be pointed to create a beam in the direction θ_g.

Whereas the speed of the individual wave-crests is the phase-velocity

$$V_p = \omega/k, \tag{143}$$

the group-velocity is

$$\boldsymbol{V}_g = \partial\omega/\partial\boldsymbol{k}, \tag{144}$$

where $\boldsymbol{k}$ is the propagation vector appearing in equation (50). Equation (144) implies that the dispersion relation must be solved to give ω as a function (k_x, k_y, k_z), and that the gradient of ω in $\boldsymbol{k}$ space must then be calculated (see Poverlein 1949).

To do this, we substitute from equation (55) into equation (50) to obtain

$$\boldsymbol{k} = (0, k_\perp, k_\parallel), \tag{145}$$

where

$$k_\parallel = k\cos\theta_p = (\omega/c)\, n\cos\theta_p \tag{146}$$

and

$$k_\perp = k\sin\theta_p = (\omega/c)\, n\sin\theta_p. \tag{147}$$

These are the components of the propagation vector parallel and perpendicular to the direction of the imposed magnetic field. We may now rewrite the dispersion relation (65) as

$$\alpha(ck/\omega)^4+\gamma(ck/\omega)^2+\epsilon=0, \tag{148}$$

where, on substituting into equations (66), (67) and (68) for $\sin\theta_p$ in terms of $k_\perp$ from equation (147), we have

$$\alpha=(1+\kappa_L)-(\kappa_L-\kappa_T)(k_\perp/k)^2, \tag{149}$$

$$\gamma=-2(1+\kappa_L)(1+\kappa_T)+\{(1+\kappa_T)(\kappa_L-\kappa_T)-\kappa_H^2\}(k_\perp/k)^2, \tag{150}$$

$$\epsilon=(1+\kappa_L)\{(1+\kappa_T)^2+\kappa_H^2\}. \tag{151}$$

By substituting from equations (149), (150) and (151), and using the fact that $k^2=k_\parallel^2+k_\perp^2$, it follows that the dispersion formula (148), if expressed as a relation between ω, $k_\parallel$ and $k_\perp$, is

$$\begin{aligned}c^4(k_\parallel^2+k_\perp^2)\{(1+\kappa_L)k_\parallel^2+(1+\kappa_T)k_\perp^2\}-c^2\omega^2[(1+\kappa_T)(1+\kappa_L)(2k_\parallel^2+k_\perp^2)\\+\{(1+k_T)^2+\kappa_H^2\}k_\perp^2]+\omega^4(1+\kappa_L)\{(1+\kappa_T)^2+\kappa_H^2\}=0.\end{aligned} \tag{152}$$

We may regard this as an equation giving ω as a function of $k_\parallel$ and $k_\perp$, and proceed to differentiate the equation partially with respect to $k_\parallel$ and $k_\perp$, thereby calculating $\partial\omega/\partial k_\parallel$ and $\partial\omega/\partial k_\perp$, which are the components of the group-velocity parallel and perpendicular to the direction of the imposed magnetic field.

In general, it is necessary to ensure that the coordinates of the point at which the field is being evaluated are real, and that the time at which the field is being evaluated is real. If collisions are taken into account, this results in the appropriate values of $k_\parallel$, $k_\perp$ and ω being complex. However, if collisions are neglected, there is a sharp distinction between pass-bands and stop-bands, and in the former V_g, θ_g, $k_\parallel$, $k_\perp$ and ω are all real. For each frequency in a pass-band, therefore, we may plot a polar diagram of V_g as a function of θ_g, with θ_p expressed as a parameter along the curve.

Let us examine the results of performing this type of calculation. The upper halves of figures 6*a* and *b* show that there are five pass-bands to discuss:

(i) $\omega>\omega_{C2}$, horizontal shading, the X wave;

(ii) $\omega_{C1}<\omega<\omega_{\infty 2}$, horizontal shading, the X wave;

(iii) $\omega<\mathrm{Min}\,(\omega_N,\omega_{Me})$, horizontal shading at the lower frequencies and vertical shading at the higher frequencies, the whistler wave;

(iv) $\omega>\omega_N$, vertical shading, the O wave;

(v) $\omega<\omega_{Mi}$, vertical shading, the O wave.

12. Group propagation of the X wave in the pass-band $\omega>\omega_{C2}$

At angular frequencies large compared with ω_{C2} the magnetoplasma has virtually no influence on propagation of the X wave, and the group velocity in all directions relative to the imposed magnetic field is c. A short pulse emitted from a point-source S in the magnetoplasma would therefore be found, at unit time later, at a sphere of radius c, centre S, as indicated in figure 8 ($\omega\gg\omega_{C2}$).

If, however, the angular frequency is not large compared with ω_{C2}, then the group-velocity along the imposed magnetic field is a little less than that across the field, and both are less than c. Consequently a short pulse emitted from a point-source at S is to be found, at unit time later, in the neighbourhood of a slightly non-spherical surface that lies entirely within the sphere of radius c

as shown in figure 8. The curve shown in figure 8 must be rotated about the imposed magnetic field $\boldsymbol{B}_0$ in order to picture the surface indicating the location of the pulse at unit time. The length of the radius vector at angle θ_g to $\boldsymbol{B}_0$ gives the corresponding value of V_g. An arrow drawn at the tip of such a radius vector in figure 8 makes an angle θ_p with $\boldsymbol{B}_0$, and therefore gives the direction in which a broadside antenna must be faced in order to produce an X wave beam along the selected radius vector. It will be noticed that the arrows in figure 8 are not quite radial, showing that the broadside antenna must be pointed in a direction slightly different from that desired for the beam, except for beams parallel and perpendicular to $\boldsymbol{B}_0$. Uniform rotation of the antenna about an axis perpendicular to $\boldsymbol{B}_0$. produces a rotation of the beam that is not quite uniform. As the antenna turns from the longitudinal to the transverse direction, so does the beam; but in intermediate positions the direction of the beam lags slightly behind that of the antenna.

As ω is reduced towards ω_{C2}, the group velocity in all directions is reduced. It tends to zero at the cut-off frequency ω_{C2} of the pass-band, and with further reduction of ω one enters a stop-band.

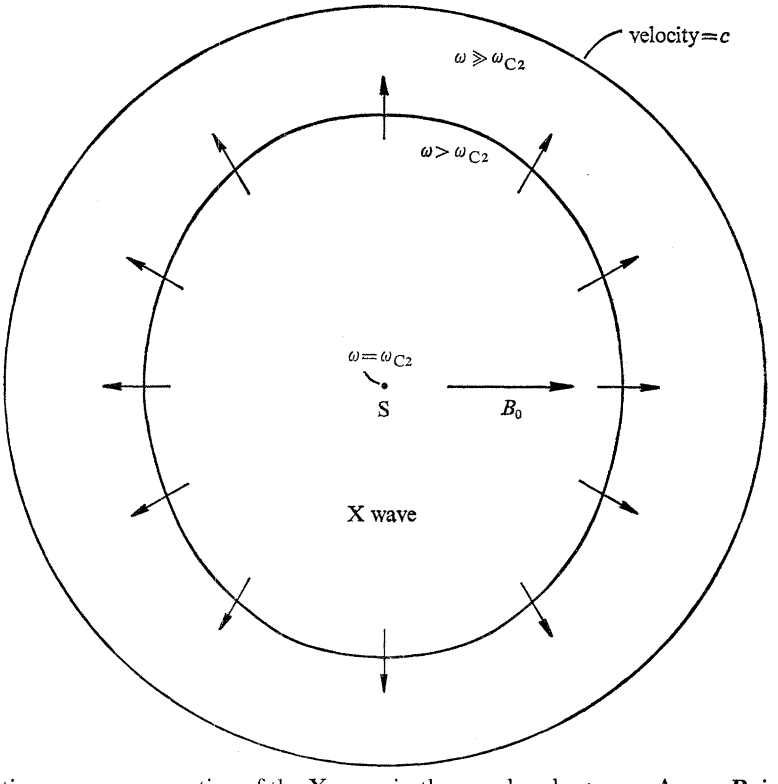

FIGURE 8. Illustrating group propagation of the X wave in the pass-band $\omega > \omega_{C2}$. Arrow $\boldsymbol{B}_0$ indicates direction of the imposed magnetic field. Other arrows indicate directions of phase propagation.

13. GROUP PROPAGATION OF THE X WAVE IN THE PASS-BAND $\omega_{C1} < \omega < \omega_{\infty 2}$

The behaviour of the X wave in this band is shown in figures 9 and 10 for $\omega_N < \omega_{Me}$. Figure 9 refers to the portion of the band above ω_{Me} and figure 10 to that below ω_{Me}. Figure 9 shows that, near the top of the band, the surface of revolution occupied after unit time by a short pulse emitted from a point-source at S is not the slightest approximation to a sphere. There is a substantial range of directions (around the lines of flux of the imposed magnetic field) in which the beam cannot be pointed no matter how the antenna is oriented. Moreover, the arrows on the

curve in figure 9 indicating how θ_p varies with θ_g reveal that no arrow points along the lines of flux of the imposed magnetic field. If a large broadside antenna designed to generate only the X wave at the frequency appropriate to figure 9 is pointed along $\boldsymbol{B}_0$, the input impedance to it is reactive and the antenna does not radiate. If the antenna is now turned counter clockwise about an axis perpendicular to $\boldsymbol{B}_0$, the antenna starts to radiate when it has turned through an angle of about 20°. But the direction of the beam is then perpendicular to the direction of the antenna;

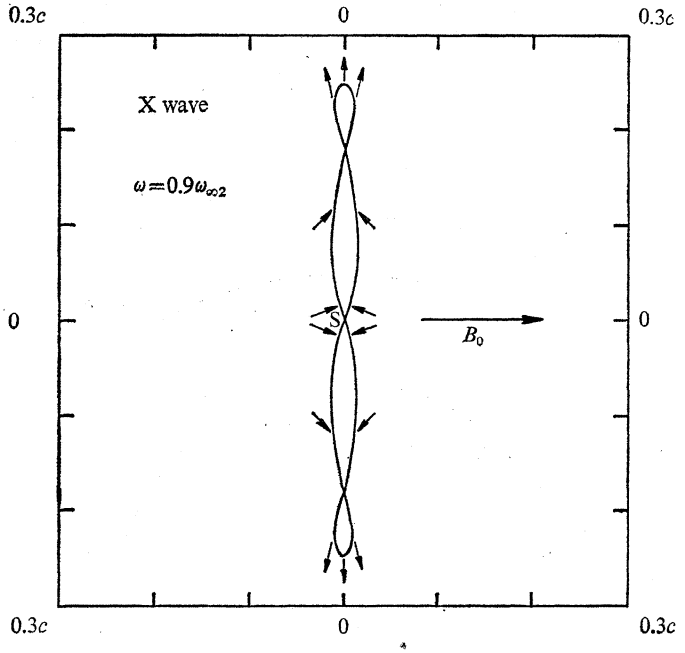

FIGURE 9. Illustrating group propagation of the X wave in the upper part of the pass-band $\omega_{C1} < \omega < \omega_{\infty 2}$. Arrow $\boldsymbol{B}_0$ indicates direction of the imposed magnetic field. Other arrows indicate directions of phase propagation. $\omega_N^2 = 10^{-\frac{1}{2}}\omega_{Me}^2$, $\omega_{Mi} = 10^{-4}\omega_{Me}$, no collisions.

the beam is pointing at an angle of about 110° to $\boldsymbol{B}_0$. Moreover the group velocity is then very small. As the antenna continues to rotate in the counterclockwise direction, the group velocity increases and the beam turns slowly in the clockwise direction, passing through $\theta_g = 90°$ when the antenna angle θ_p is about 60°. With continued rotation of the antenna in the counterclockwise direction, the beam first continues to rotate clockwise, then comes to rest, and finally starts rotating counterclockwise. When the antenna has reached the transverse position $\theta_p = 90°$, so has the beam reached the transverse position $\theta_g = 90°$. Continuous rotation of a broadside antenna through 360° results in a sector scan of the beam, first about $\theta_g = 90°$ and then about $\theta_g = 270°$. As the beam becomes folded flat against the face of the antenna, the group velocity drops to zero and the antenna passes into a non-radiating condition (stop-band behaviour).

As the angular frequency increases to the top of the band at $\omega_{\infty 2}$, the group velocity even in the transverse direction drops to zero, and one then passes into an X-wave stop-band for all directions of propagation.

If, on the other hand, one moves downwards in frequency, figure 9 becomes converted into the form shown in the top left hand corner of figure 10. Radiation of the X wave in all directions in the magnetoplasma is now possible, but uniform rotation of a broadside antenna produces very non-uniform rotation of the beam. Figure 10 shows the various changes in behaviour that take place before the group velocity tends to zero at the bottom of the band ($\omega = \omega_{C1}$).

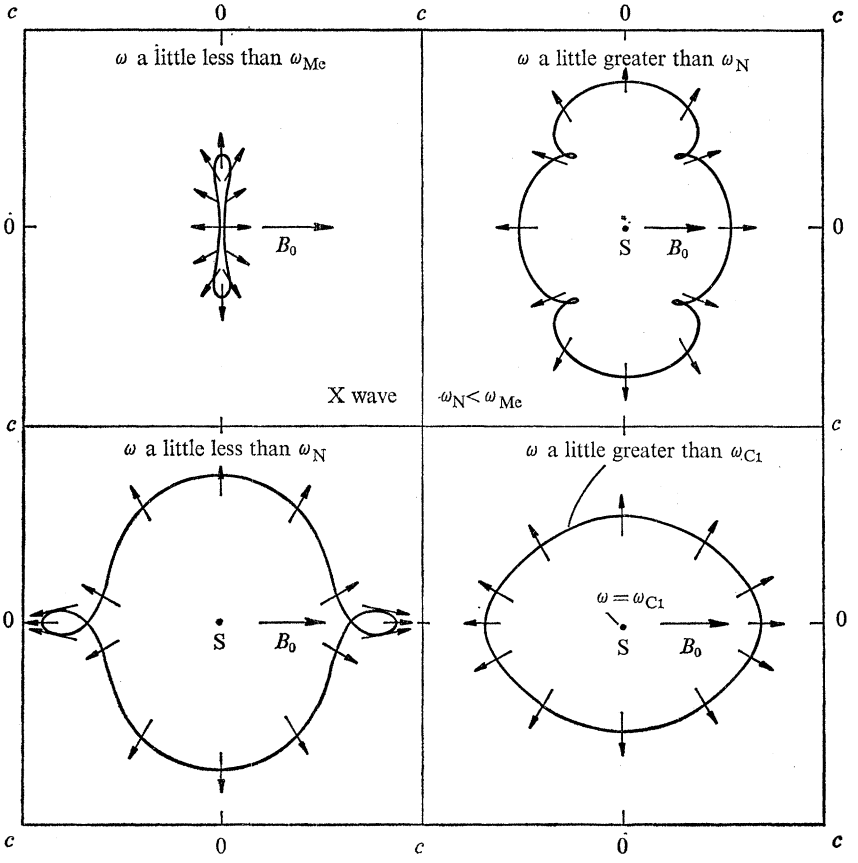

FIGURE 10. Illustrating group propagation of the X wave in the lower part of the pass-band $\omega_{C1} < \omega < \omega_{\infty 2}$. Arrow $\boldsymbol{B}_0$ indicates direction of the imposed magnetic field. Other arrows indicate directions of phase propagation. $\omega_N^2 = 10^{-\frac{1}{2}}\omega_{Me}^2$, $\omega_{Mi} = 10^{-4}\omega_{Me}$, no collisions.

14. GROUP PROPAGATION OF THE WHISTLER WAVE IN THE PASS-BAND $\omega <$ Min (ω_N, ω_{Me})

Following Gendrin (1960), this is illustrated in figure 11 for the upper part of the band where the radio approximation is reasonably good. The behaviour for the lower part of the band, where the hydromagnetic approximation is reasonably good, is shown in figure 12.

In the top left hand diagram of figure 11 it should be noted that transmission transverse to $\boldsymbol{B}_0$ is not possible. At this frequency the beam of a broadside antenna with whistler wave polarization can only be aimed within a certain cone of directions around the lines of flux of the imposed magnetic field no matter how the antenna is oriented. Moreover, the arrows in the upper half of this diagram all slope downwards, while in the lower half they all slope upwards. This means that, when a broadside antenna with whistler wave polarization is turned away from $\boldsymbol{B}_0$ in the counter-clockwise direction, the beam turns in the clockwise direction. Counter-rotation of the antenna and the beam continues until the beam is folded flat against the face of the antenna, when radiation ceases. Hence, for the top left hand diagram in figure 11, continuous rotation of the antenna through 360° about an axis perpendicular to $\boldsymbol{B}_0$ results in a sector scan of the beam, first about $\theta_g = 0°$ and then about $\theta_g = 180°$. In the sectors for which radiation takes place, rotation of the beam always occurs in the direction opposite to rotation of the antenna.

As we move down the frequency band, the angle of the radiation sectors decreases, and the dumb-bell shaped surface of revolution indicated in the top left hand diagram of figure 11 develops points on its axis of symmetry, and then lobes, leading to the surface of revolution indicated in the top right hand diagram of figure 11. Continuous rotation of a broadside antenna around an axis perpendicular to $\boldsymbol{B}_0$ now produces a double sector scan first about $\boldsymbol{B}_0$ and then about $-\boldsymbol{B}_0$. If the antenna is pointed along $\boldsymbol{B}_0$, the beam is along $\boldsymbol{B}_0$; but when the antenna has turned to about $\theta_p = 60°$, the beam is back again in the direction $\theta_g = 0°$, and it then proceeds to negative values of θ_g.

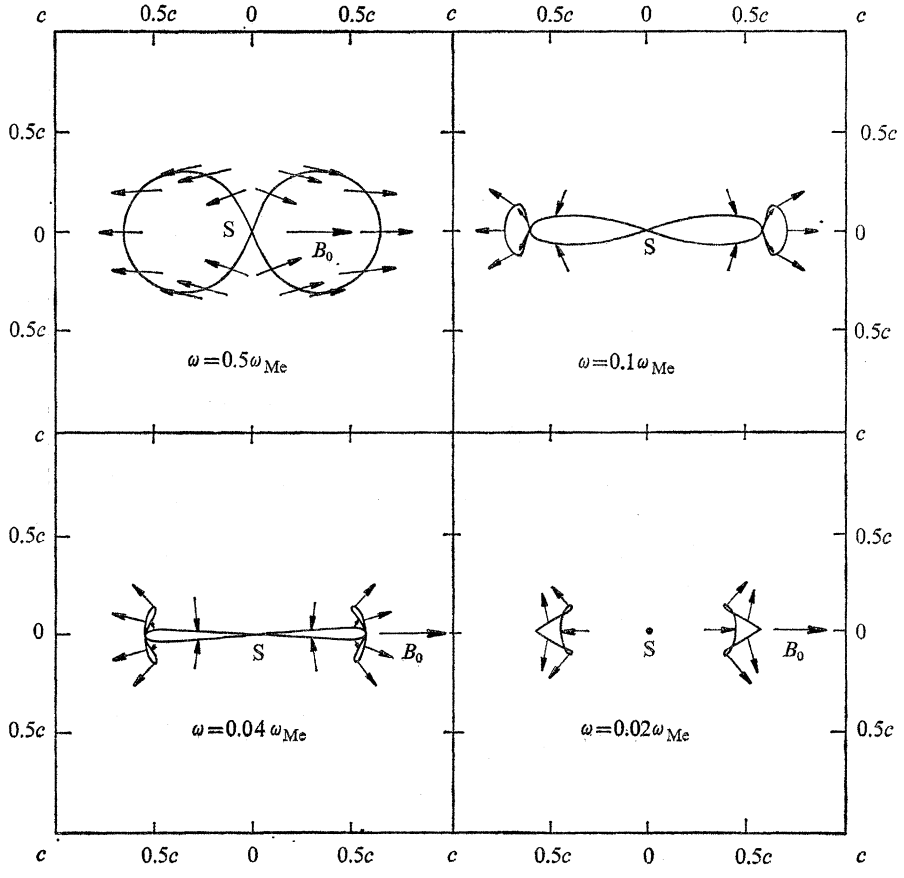

FIGURE 11. Illustrating group propagation of the whistler wave in the upper part of the pass-band $\omega <$ Min (ω_N, ω_{Me}). Arrow $\boldsymbol{B}_0$ indicates direction of the imposed magnetic field. Other arrows indicate directions of phase propagation. $\omega_N^2 = 10^{-\frac{1}{2}}\omega_{Me}^2$, $\omega_{MI} = 10^{-4}\omega_{Me}$, no collisions.

Although the top left hand diagram in figure 11 was peculiar in that the beam rotated in the opposite direction to the antenna, it was simple in the sense that, in any direction of radiation, a single emitted pulse led to single radiated pulse with a specific group velocity. But for the top right hand diagram of figure 11, there are directions in which three pulses are radiated, each with its own group velocity. For the direction $\theta_g = 0°$, two of these pulses, corresponding roughly to $\theta_p = \pm 60°$, have equal group-velocities, and the third pulse, corresponding to $\theta_p = 0°$, has a larger group-velocity. However, as we move down the frequency band, all three of these group velocities for $\theta_g = 0°$ become equal as shown in the bottom left hand diagram of figure 11, and then the group velocity for $\theta_p = 0°$ becomes the smaller one as shown in the bottom right hand

diagram. In this diagram two pairs of nearly coincident lines joining S to the conical points of the surfaces of revolution have been omitted; they represent pulses that are highly dispersed, and that would also be substantially attenuated if collisions were taken into account.

The top left hand diagram of figure 12 is identical with the bottom right hand diagram of figure 11. However, velocities in figure 12 are marked, not in terms of c but in terms of the ionic Alfvén velocity A_i; in addition, the angular frequencies are referred, not to the electronic gyrofrequency ω_{Me}, but to the lower hybrid resonant frequency $\omega_{\infty 1}$ and the ionic gyrofrequency ω_{Mi}. Figure 12 shows that, as one moves down the band through the lower hybrid resonant frequency, one encounters a situation in which radiation can take place in all directions. At frequencies small compared with the ionic gyrofrequency, the whistler wave becomes the omnidirectional Alfvén wave, for which the group velocity in all directions is A_i.

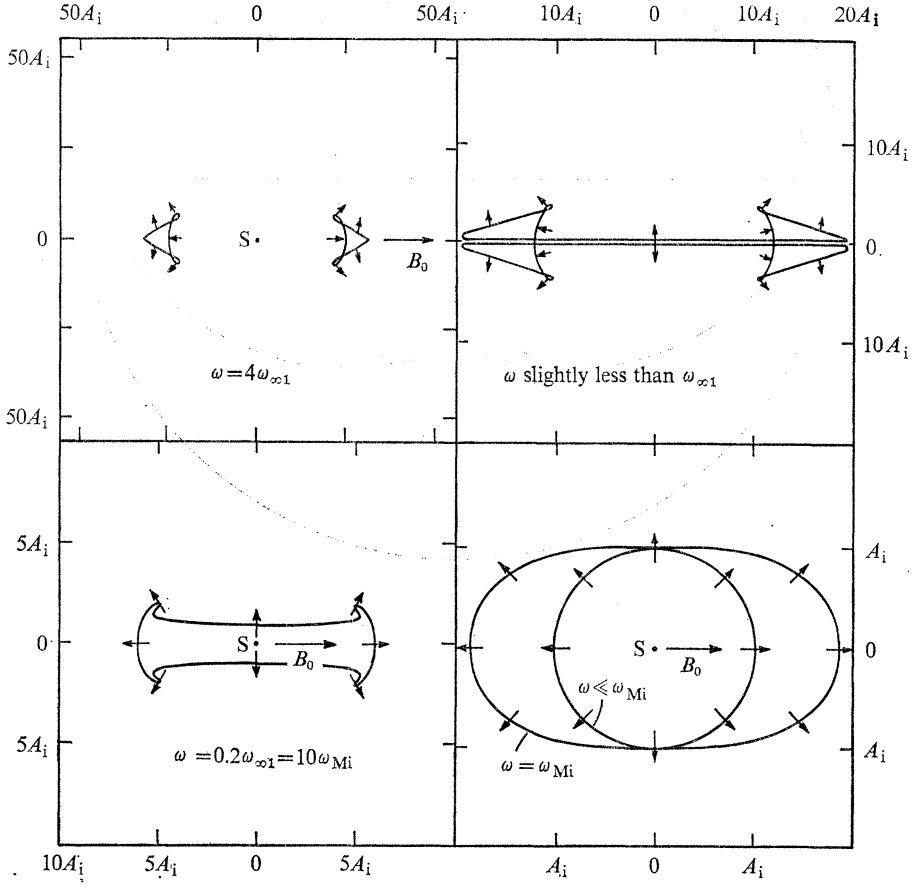

FIGURE 12. Illustrating group propagation of the whistler wave in the lower part of the pass-band $\omega <$ Min (ω_N, ω_{Me}). Arrow $\boldsymbol{B}_0$ indicates direction of the imposed magnetic field. Other arrows indicate directions of phase propagation. $\omega_N^2 = 10^{-\frac{1}{2}}\omega_{Me}^2$, $\omega_{Mi} = 10^{-4}\omega_{Me}$, no collisions.

15. GROUP PROPAGATION OF THE O WAVE IN THE PASS-BAND $\omega > \omega_N$

This is illustrated in figure 13. For sufficiently high frequencies the magnetoplasma has virtually no influence on propagation of the O wave, and we have a sphere of radius c. This contracts as the frequency is reduced, but it does not contract to a point at the cut-off frequency ω_N of the band. Instead, it contracts to a line along the direction of $\boldsymbol{B}_0$ as indicated in figure 13.

We thus see that the high pass-band for the O wave actually behaves in a more unusual manner than the high pass-band for the X wave (figure 8). Nevertheless the cut-off frequency ω_N for the O wave is independent of the imposed magnetic field, whereas this is not true for the cut-off frequency ω_{C2} for the X wave (equation 97). Moreover, for the O wave in figure 13, the group velocity in the direction transverse to $\boldsymbol{B}_0$ (that is, in the vertical direction in the diagram) is the same as it would be in the absence of the imposed magnetic field.

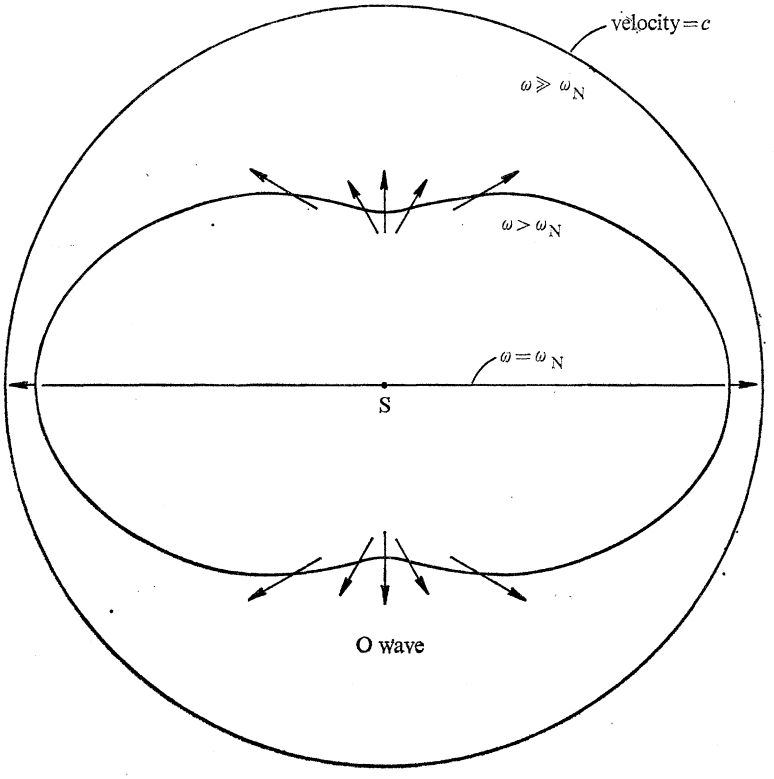

FIGURE 13. Illustrating group propagation of the O wave in the pass-band $\omega > \omega_N$. Arrows indicate directions of phase propagation. The imposed magnetic field $\boldsymbol{B}_0$ is horizontal.

16. GROUP PROPAGATION OF THE O WAVE IN THE PASS-BAND $\omega < \omega_{M1}$

This is illustrated in figure 14, where the succession of diagrams from top to bottom constitutes progression down the band from an angular frequency close to ω_{M1} to an angular frequency small compared with ω_{M1}. Let us look first at the second of these diagrams.

After rotation round $\boldsymbol{B}_0$, this diagram represents a pair of conical-shaped surfaces corresponding to group velocities a little less than the ionic Alfvén velocity A_1. The beam is pointed more or less in the direction $\boldsymbol{B}_0$, or $-\boldsymbol{B}_0$, regardless of the direction in which the antenna is pointed. Continuous rotation of a broadside antenna through 360° about an axis perpendicular to $\boldsymbol{B}_0$ would result in a sector scan of the beam about $\theta_g = 0°$ followed by a sector scan about $\theta_g = 180°$.

As we move upwards in frequency, the group velocity tends to zero at the top of the band ($\omega = \omega_{M1}$). As we move downwards in frequency the angle of the sector scans diminishes towards zero.

Let us consider the interpretation of figure 14 in circumstances where a point source, rather than a broadside antenna, is placed in the magnetoplasma at S, polarized so as to generate only

the O wave in the band $\omega < \omega_{\mathrm{MI}}$. We see that, when $\omega \ll \omega_{\mathrm{MI}}$, radiation is confined to narrow cones around the directions $\pm \boldsymbol{B}_0$. The magnetoplasma may be said to convert the point-source S into a pair of end-fire antennae that point in the two opposite directions $\pm \boldsymbol{B}_0$. Moreover, they are end-fire antennae that have the unusual property that their beam-angle becomes smaller as the frequency is reduced. At the same time the length of the guidance-zone (or Fresnel zone) for the end-fire antennae increases, and tends to infinity as the frequency tends to zero.

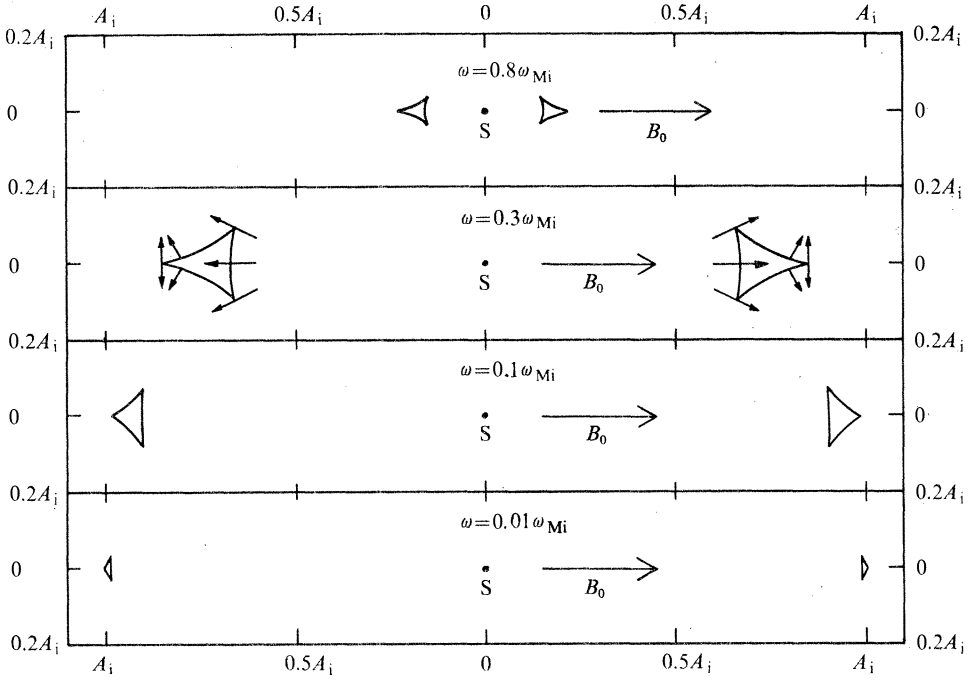

FIGURE 14. Illustrating group propagation of the O wave in the pass-band $\omega < \omega_{\mathrm{MI}}$. Arrow $\boldsymbol{B}_0$ indicates direction of imposed magnetic field. Other arrows indicate directions of phase propagation. $\omega_{\mathrm{N}}^2 = 10^{-\frac{1}{2}}\omega_{\mathrm{Me}}^2$, $\omega_{\mathrm{Mi}} = 10^{-4}\omega_{\mathrm{Me}}$, no collisions.

17. PASS- AND STOP-BANDS OF IONIZATION DENSITY

So far we have considered pass- and stop-bands of wave-frequency for a magnetoplasma having a fixed ionization density and a fixed imposed magnetic field. However, it is possible to let the frequency be fixed and to let the ionization density or the imposed magnetic field vary, or both. Particular interest attaches to curves showing n^2 as a function of ω_{N}^2 (proportional to ionization density) for a fixed wave-frequency and a fixed imposed magnetic field. These were the original dispersion curves employed for the ionosphere to study the propagation of vertically incident waves. The angle θ_{p} is then the angle that the Earth's magnetic field makes with the vertical; it varies from 0° at a magnetic pole to 90° at the magnetic equator.

Curves of this type, taken from the early work of Ratcliffe (1933), are shown in figures 15 and 16 for frequencies of twice and half the electronic gyrofrequency. For these frequencies the radio approximation, $\omega \gg (\omega_{\mathrm{Me}}\omega_{\mathrm{Mi}})^{\frac{1}{2}}$, is adequate. The variation of n^2 with ω_{N}^2 for polar regions is marked $\theta_{\mathrm{p}} = 0°$ and that for the equator is marked $\theta_{\mathrm{p}} = 90°$. For intermediate latitudes the curves run through the shaded regions, vertical shading referring to the O wave and horizontal

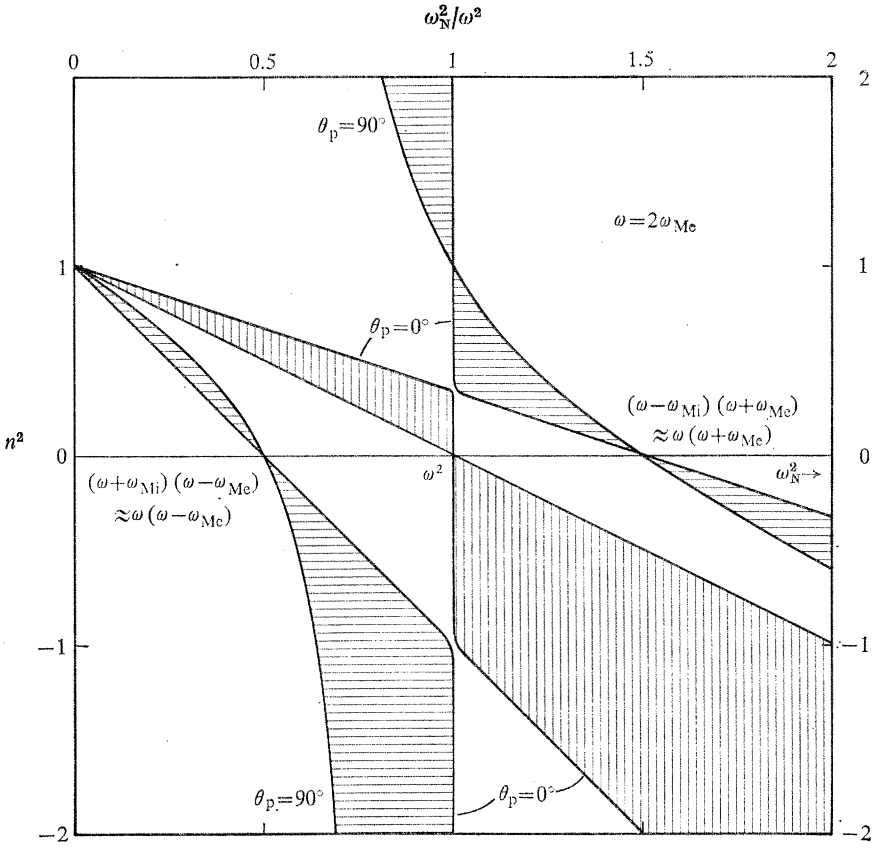

FIGURE 15. Variation of n^2 with $\omega_N^2(\propto N)$ for O wave (vertical shading) and X wave (horizontal shading). $\omega > \omega_{Me}$, no collisions.

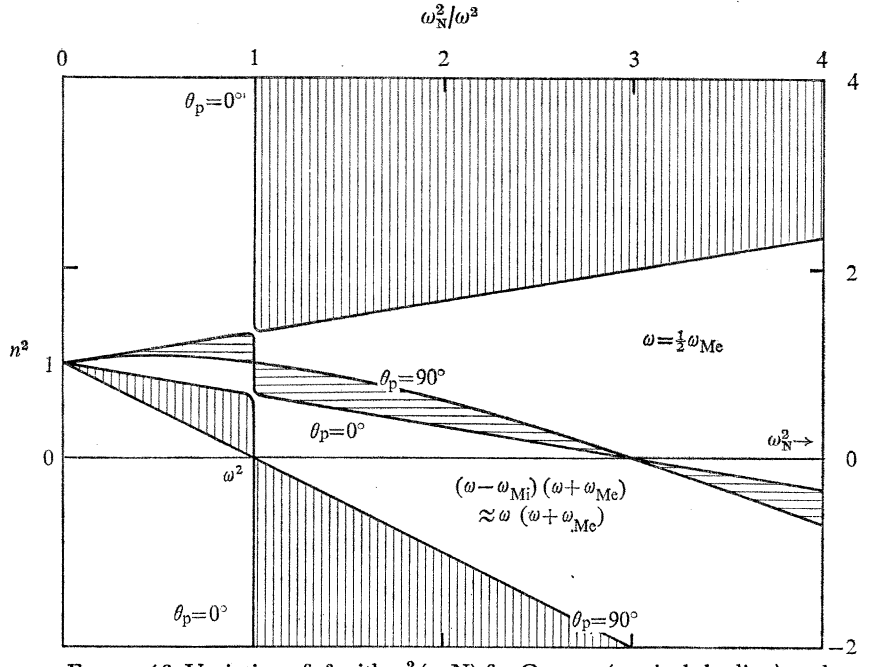

FIGURE 16. Variation of n^2 with $\omega_N^2(\propto N)$ for O wave (vertical shading) and X wave (horizontal shading). $(\omega_{Me}\omega_{Mi})^{\frac{1}{2}} < \omega < \omega_{Me}$, no collisions.

shading to the X wave. The upper half of figure 15 illustrates the fact that, at wave-frequencies above the electronic gyrofrequency, there is a pass-band of ionization for the O wave given by

$$\omega_N^2 < \omega^2 \tag{153}$$

and a pass-band of ionization for the X wave given by

$$\omega_N^2 < (\omega + \omega_{Mi})(\omega - \omega_{Me}). \tag{154}$$

Figure 16 illustrates the fact that, between the two gyrofrequencies, there is a pass-band of ionization for the O wave given by

$$\omega_N^2 < \omega^2 \tag{155}$$

and a pass-band of ionization for the X wave given by

$$\omega_N^2 < (\omega - \omega_{Mi})(\omega + \omega_{Me}). \tag{156}$$

Both in figure 15 and in figure 16 there is an additional pass-band of ionization. In figure 16, an O-wave curve for $0° < \theta_p < 90°$ starting from $n^2 = 1$ at $\omega_N^2 = 0$ first passes, via the vertically shaded region, through $n^2 = 0$ at $\omega_N^2 = \omega^2$, continues to $n^2 = -\infty$ in the region $\omega_N^2 > \omega^2$, and then reappears at $n^2 = +\infty$. From here to infinite ionization density there is a pass-band of ionization corresponding to the whistler wave. Moreover when $\omega_N^2 \gg \omega^2$ we may employ the hydromagnetic approximation.

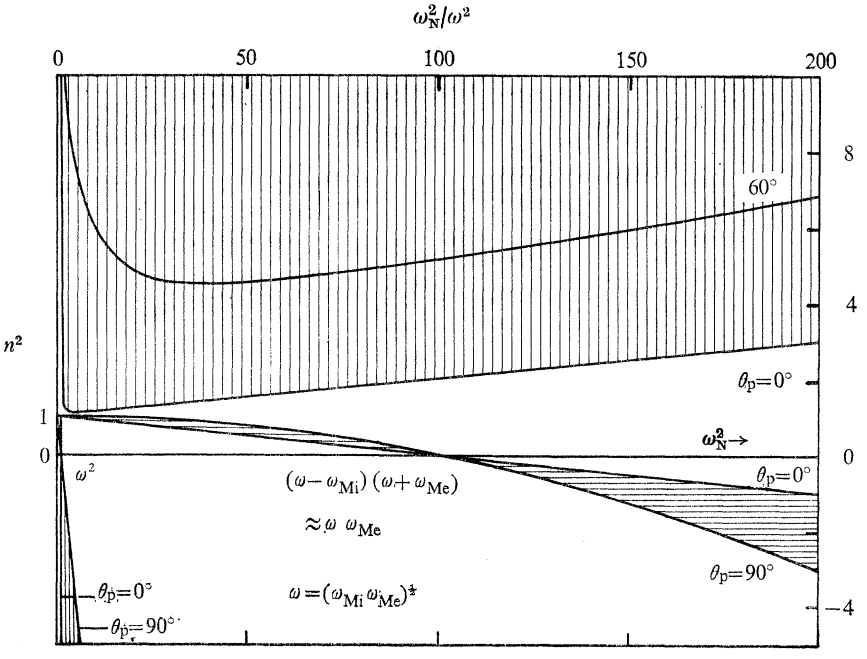

FIGURE 17. Variation of n^2 with $\omega_N^2 (\propto N)$ for O wave (vertical shading) and X wave (horizontal shading). $\omega = (\omega_{Me}\omega_{Mi})^{\frac{1}{2}}$, no collisions.

The upper boundary of an ionization pass-band that extends down to zero ionization density gives, for the ionosphere, the level of reflexion of waves incident vertically from below. These critical ionization densities decrease as the frequency decreases. Figure 16 illustrates the fact that, for $\omega_{Mi} \ll \omega \ll \omega_{Me}$, the critical ionization density decreases proportional to ω^2 for the O wave, but proportional to ω for the X wave. The ratio of the first of these critical ionization densities to the second is of the order of 10^{-2} when the wave-frequency has decreased to the

geometric mean of the gyrofrequencies as shown in figure 17. At this frequency the radio approximation is no longer satisfactory, but its inadequacy only occurs at ionization densities greater than those appearing in figure 17. Moreover, when $\omega_N^2 \gg \omega^2$, we may use the hydromagnetic approximation.

With further decrease of ω, the ratio of the critical ionization density for the O wave to that for the X wave decreases to the order of 10^{-4} at a frequency only a few times the ionic gyrofrequency. For lower frequencies, however, the fact $(\omega - \omega_{Mi})$ on the right hand side of inequality (156) becomes important and causes the critical ionization density for the X wave to plunge down to zero at $\omega = \omega_{Mi}$. Figure 18 shows the situation just before the critical ionization density for the X wave crosses that for the O wave.

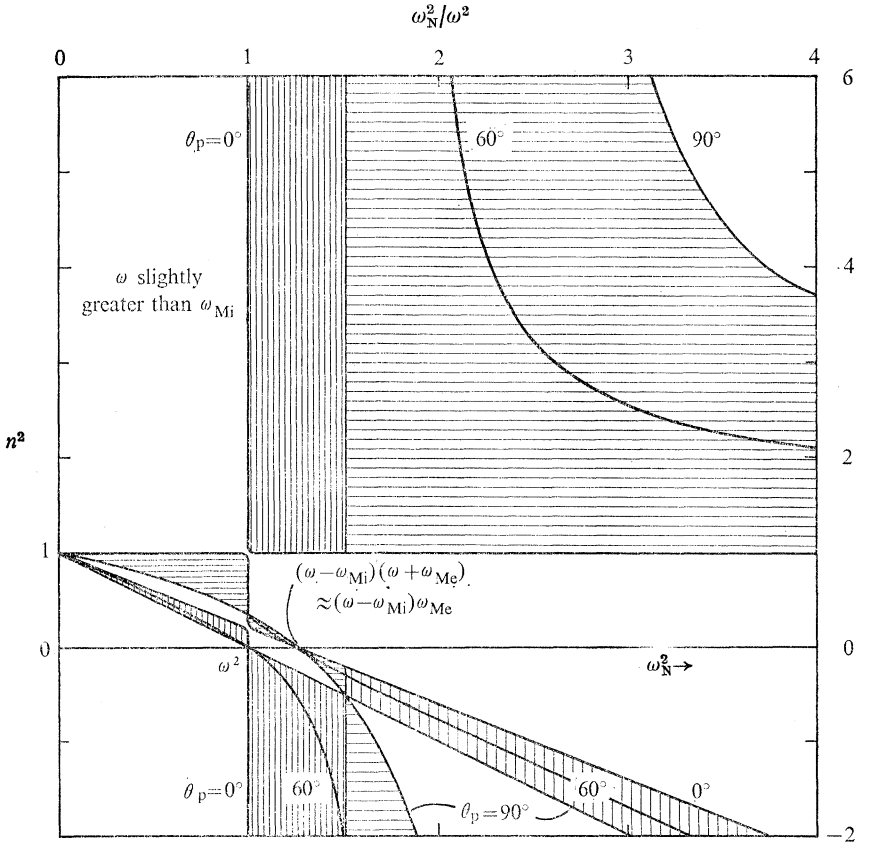

FIGURE 18. Variation of n^2 with $\omega_N^2 (\propto N)$ for O wave (vertical shading) and X wave (horizontal shading). $\omega_{Mi} < \omega < (\omega_{Me}\omega_{Mi})^{\frac{1}{2}}$, no collisions.

Figure 18 exhibits two features of the (n^2, ω_N^2) curves that are characteristic of wave-frequencies between the ionic gyrofrequency and the geometric mean of the two gyrofrequencies. First, the $\theta_p = 90°$ curve for the X wave has an infinity for a positive value of ω_N^2. Secondly, the O and X wave curves for $\theta_p = 90°$ cross, resulting in the whistler wave having the O name below a certain ionization density (vertical shading) and the X name above it (horizontal shading). As in figures 6*a* and *b*, this change of name is conveniently circumvented by using the whistler nomenclature.

As ω decreases below ω_{Mi}, the critical ionization for the X wave corresponding to

$$\omega_N^2 = (\omega - \omega_{Mi})(\omega + \omega_{Me}) \qquad (157)$$

becomes negative and loses significance. On the other hand, that for the O wave corresponding to

$$\omega_N^2 = \omega^2 \tag{158}$$

retains significance, although the character of the significance frequently has to be carefully examined. Figure 19 shows the situation for a frequency equal to half the ionic gyrofrequency. The diagram is drawn in two parts with ionization scales differing by four powers of ten; the horizontal scale in the upper diagram is proportional to the square of essentially the electronic plasma-frequency, whereas that in the lower diagram is proportional to the square of the ionic plasma-frequency. The lower diagram is drawn by using the hydromagnetic approximation. The upper diagram shows, for the O wave, how the lower diagram needs to be modified for abscissae between 0 and 3×10^{-4}.

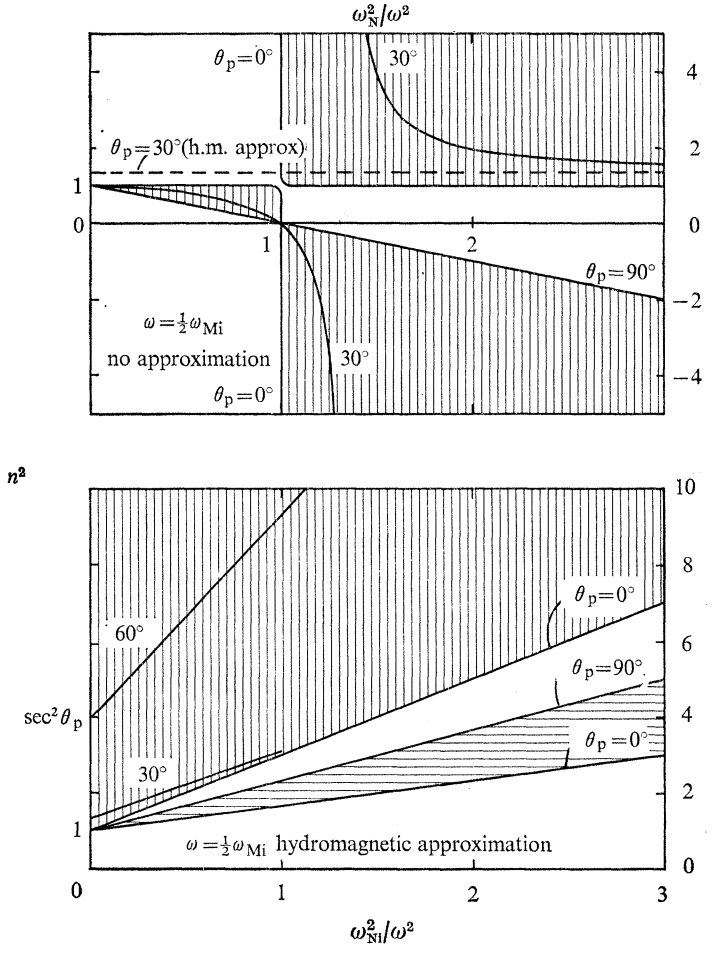

FIGURE 19. Variation of n^2 with ionization density for O wave (vertical shading) and X wave (horizontal shading), $\omega < \omega_{Mi}$. Upper diagram shows the behaviour of the O wave for abscissae in the lower diagram between 0 and 3×10^{-4}. $\omega_{Mi} = 10^{-4}\omega_{Me}$, no collisions.

Looking first at the lower diagram in figure 19, we see that, for all values of θ_p, n^2 for the X wave increases steadily from unity; all positive ionization densities constitute a pass-band for the X wave for all values of θ_p. For the O wave it would appear from the lower diagram in figure 19 that it is also true that all positive ionization densities constitute a pass-band for all values of θ_p. However, we notice that, except for $\theta_p = 0°$, there is a discontinuity of n^2 at zero ionization

density. How this apparent discontinuity comes about is shown in the upper diagram. Looking at the curve for $\theta_p = 30°$, we see that the hydromagnetic approximation for the O wave in the lower diagram is satisfactory down to abscissae somewhat greater than 10^{-4}, and that n^2 then passes to unity via an infinity, thereby creating at $\omega_N^2 = \omega^2$ the critical ionization density expected for the O wave in accordance with equation (158).

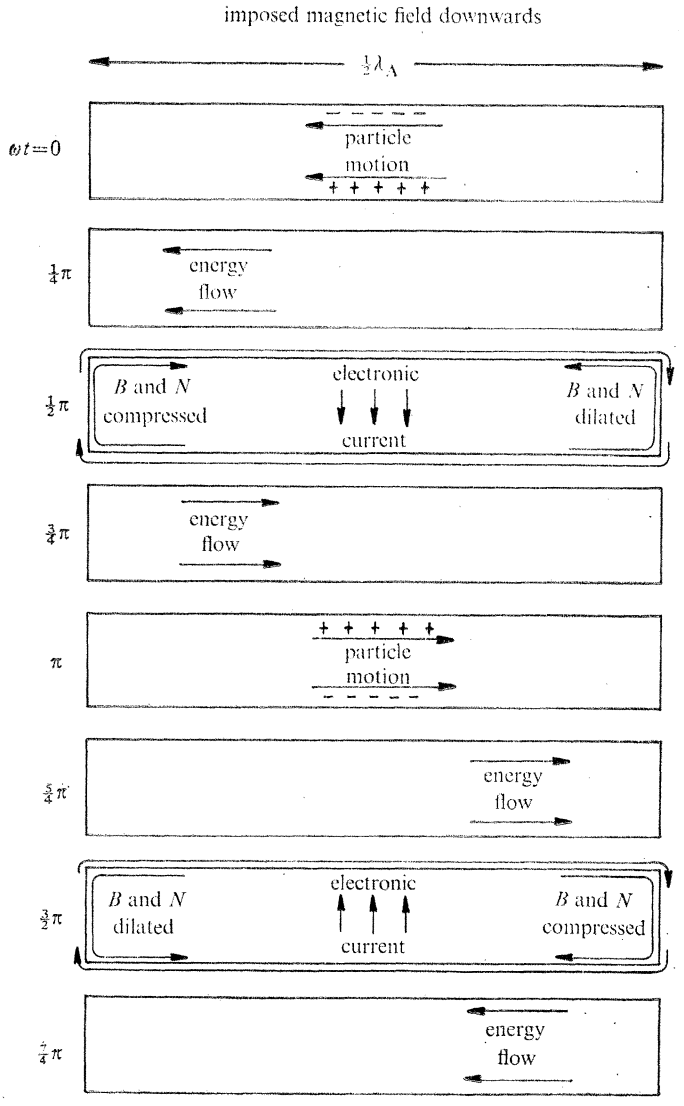

FIGURE 20. Behaviour of a transverse Alfvén wave in a resonator composed of a half wavelength of perfectly conducting strip transmission-line short-circuited at both ends and filled with plasma.

In applying figures 15–19 to vertical propagation in a horizontally stratified ionosphere, the possibility has to be borne in mind that tunnelling may take place through an ionization stop-band. This can occur either because the gradient of ionization is too great, or because collisions are important, or because the ionosphere contains substantial irregularities of ionization density. For example, the O wave curves in the lower diagram of figure 19, although based on an approximation, frequently give a better description than the upper diagram of what would be

likely to happen when entering the ionosphere vertically at a frequency less than the ionic gyrofrequency. Consider, for example, a latitude corresponding to $\theta_p = 30°$, and for simplicity let us neglect the effect of collisions or of irregularities of ionization density. For reasons of ionization gradient alone, the O wave could easily tunnel completely through the ionization stop-band shown in the upper diagram, responding only to the net change in n^2 between an ionization density small compared with that for the zero of n^2 and an ionization density somewhat above that for the infinity of n^2. This is the discontinuity in n^2 shown in the lower diagram at zero ionization density. However, the discontinuity should be placed, not at zero ionization density, but at an ionization density of the order of magnitude involved for the stop-band in the upper diagram.

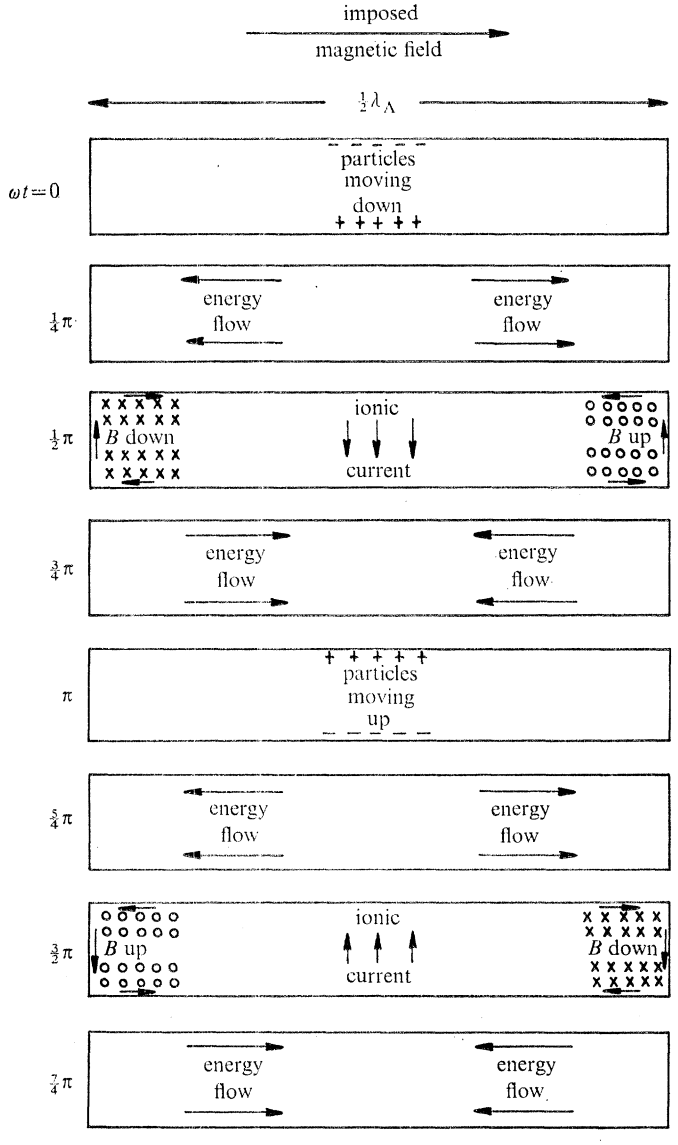

FIGURE 21. Behaviour of a longitudinal Alfvén wave in a resonator composed of a half wavelength of perfectly conducting strip transmission-line short-circuited at both ends and filled with plasma.

18. The concept of frozen-in magnetic field

Hitherto we have kept the oscillatory magnetic field of the wave separate from the steady imposed magnetic field. However, there are circumstances in which an advantage is to be gained by combining the two and thinking in terms of the resultant magnetic field. This occurs when collisions are unimportant, and when one is discussing Alfvén waves (1942*a*, *b*, 1950). To a useful degree of approximation the resultant magnetic field is then frozen in the plasma, so that the tubes of resultant magnetic field have the same coherent motion as the charged particles, and each tube retains its own plasma.

As an example, let us consider propagation of the X wave transverse to the imposed magnetic field at a frequency small compared with the ionic gyrofrequency in circumstances when collisions are negligible. This is included in the discussion of § 8 and figure 4, and involves propagation with the ionic Alfvén velocity A_1. To visualize the wave, let us suppose that propagation is taking place in a perfectly conducting strip transmission-line for which fringing may be neglected. The strips are perpendicular to the electric field, that is, to the x axis in § 8, and lie along the y axis, with the imposed magnetic field along the z axis. Let us use a half wavelength of such a transmission-line, short-circuited at both ends, as a resonator in the manner illustrated in figure 20 (λ_A is the Alfvén wavelength). In the resonator there is a plasma that is homogeneous on the average. It is rendered a magnetoplasma by a steady magnetic field perpendicular to the diagram, created by steady current flowing round the resonator used as a direct-current inductor. The eight diagrams in figure 20 show the resonant oscillation of the system at eight stages during a complete cycle.

At $\omega t = 0$ the oscillating electric field between the strips is at its maximum value, with positive charge on the lower strip and negative charge on the upper strip. Discharge takes place by means of currents round the transmission line through the terminal short-circuits, partly offset by a predominantly electronic current through the plasma. This process of discharge is at its maximum at $\omega t = \frac{1}{2}\pi$, and leads to recharging with the opposite polarity at $\omega t = \pi$. The electric field between the strips at $\omega t = 0$, combined with the steady magnetic field across the strips, implies Hall flow of the plasma parallel to the length of the resonator. This compresses the plasma at one end of the resonator at $\omega t = \frac{1}{2}\pi$ and dilates it at the other end. However, for a cold plasma, no gas pressure is involved. The increased pressure at the high density end, and the reduced pressure at the low density end, is the magnetic pressure associated with the modifications to the steady magnetic field caused by the magnetic fields associated with the discharging currents round the two ends of the line. The resonator may be described as an organ-pipe in which gas pressure has been replaced by magnetic pressure.

The concept of frozen-in magnetic field is useful for the situation shown in figure 20 for the following reason. The compression and dilation of the tubes of resultant magnetic flux at the two ends of the resonator correspond precisely to compression and dilation of the plasma, so that each tube may be regarded as preserving its own plasma. It should be noted however that, while the electrons and ions move together along the length of the resonator, they do not move together perpendicular to the strips. It is in this way that there arises the electronic current through the plasma shown in figure 20 as having its extreme values at $\omega t = \frac{1}{2}\pi, \frac{3}{2}\pi$. Without this current, the plasma would be electromagnetically indistinguishable from free space, and the velocity of propagation of Alfvén waves would be indistinguishable from c.

If the steady imposed magnetic field in figure 20 is rotated through 90° so as to be parallel to the length of the resonator, we obtain the situation illustrated in figure 21. Propagation along

the transmission-line through the magnetoplasma now involves circularly polarized Alfvén waves, which may be combined to give a linearly polarized Alfvén wave possessing Faraday rotation. However, if $\omega \ll \omega_{M1}$, the Faraday rotation along the half wavelength of the resonator is small and may be neglected. The Hall motion of the plasma for $\omega t = 0$ is still parallel to the strips but it is now perpendicular to the length of the resonator. The tube of plasma within the resonator vibrates like a violin string anchored at the two ends. Moreover the same is true of the tube of resultant magnetic flux formed by combining the oscillatory and steady magnetic fields. The two tubes move together, again creating a situation in which the resultant magnetic field is frozen in the plasma. Once more, however, the electrons and ions do not move together in the direction perpendicular to the strips; in consequence there is an oscillatory current in the plasma in this direction, predominantly ionic as indicated in figure 21.

This work was supported by the National Aeronautics and Space Aministration under Grant NGR-05-009-076, by the National Science Foundation under Grant GA-30628, and by the Office of Naval Research under Contract No. N00014-75-C-0959.

References (Booker)

Alfvén, H. 1942*a* *Ark. Mat. Astr. Fys.* **29**B, no. 2.
Alfvén, H. 1942*b* *Nature Lond.* **150**, 405.
Alfvén, H. 1950 *Cosmical electrodynamics*, Oxford: Clarendon Press.
Appleton, E. V. 1925 *Proc. Phys. Soc. Lond.* **37**, 16D.
Appleton, E. V. 1928 Papers of the General Assembly held in Washington, D.C. in October 1927, Fascicule 1, pp. 2–3. Brussels, Secretariat General of the International Union of Scientific Radio Telegraphy.
Appleton, E. V. 1932 *J. Inst. elect. Engrs* **71**, 642–650.
Aström, E. 1950 *Ark. Fys.* **2**, no. 42, 443–457.
Booker, H. G. & Dyce, R. B. 1965 *Radio Sci.* **69**D, 463–492.
Eckersley, T. L. 1935 *Nature, Lond.* **135**, 104–105.
Gendrin, R. 1960 *C.r. hebd. Seance Acad. Sci., Paris* **251**, 1085–1087.
Goubau, G. 1935 *HochfreqTech. Elektroaukust.* **46**, 37–49.
Hartree, D. R. 1931 *Proc. Camb. Phil. Soc.* **27**, 143–162.
Helliwell, R. A. 1965 *Whistlers and related ionospheric phenomena.* Stanford, California: Stanford University Press.
Lassen, H. 1927 *Elekt. Nachr Tech.* **4**, 324.
Lorentz, H. A. 1909 *The theory of electrons.* New York: Columbia University Press.
Nichols, H. W. & Schelleng, J. C. 1925*a* *Nature, Lond.* **115**, 334.
Nichols, H. W. & Schelleng, J. C. 1925*b* *Bell Syst. Tech. J.* **4**, 215–234.
Poverlein, H. 1949 *Z. angew. Phys.* **1**, 517.
Ratcliffe, J. A. 1933 *Wireless Engr* **10**, 354.
Ratcliffe, J. A. 1959 *The magnetoionic theory and its applications.* Cambridge: Cambridge University Press.
Rydbeck, O. E. H. 1948 Trans. Chalmer's University of Technology, Gothenburg, Sweden, **74**.
Storey, L. R. O. 1953 *Phil. Trans. R. Soc. Lond.* A **246**, 113–141.

PHILOSOPHICAL TRANSACTIONS OF THE ROYAL SOCIETY A MATHEMATICAL, PHYSICAL & ENGINEERING SCIENCES